Exploring Halo Substructure with Giant Stars XI

DRAFT VERSION FEBRUARY 4, 2008
Preprint typeset using LaTeX style emulateapj v. 6/22/04

EXPLORING HALO SUBSTRUCTURE WITH GIANT STARS XI: THE TIDAL TAILS OF THE CARINA DWARF SPHEROIDAL AND THE DISCOVERY OF MAGELLANIC CLOUD STARS IN THE CARINA FOREGROUND

RICARDO R. MUÑOZ[1], STEVEN R. MAJEWSKI[1], SIMONE ZAGGIA[2], WILLIAM E. KUNKEL[3], PETER M. FRINCHABOY[1], DAVID L. NIDEVER[1], DENIJA CRNOJEVIC[2], RICHARD J. PATTERSON[1,4], JEFFREY D. CRANE[1,4,6], KATHRYN V. JOHNSTON[5], SANGMO TONY SOHN[1,7], REBECCA BERNSTEIN[8], & STEPHEN SHECTMAN[6]

Draft version February 4, 2008

ABSTRACT

A new large-area Washington $M, T_2 + DDO51$ filter survey of more than 10 deg^2 around the Carina dSph galaxy reveals a *spectroscopically confirmed* power law radial density "break" population of Carina giant stars extending several degrees beyond the central King profile. Magellan telescope MIKE spectroscopy establishes the existence of Carina stars to at least 4.5 times its central King limiting radius, r_{lim} and primarily along Carina's major axis. To keep these stars bound to the dSph would require a global Carina mass-to-light ratio of $M/L \geq 6,300\ (\mathrm{M/L})_{\odot}$. The MIKE velocities, supplemented with ~ 950 additional Carina field velocities from archived VLT+GIRAFFE spectra with $r \lesssim r_{lim}$, demonstrate a nearly constant Carina velocity dispersion (σ_{v}) to just beyond $r = r_{lim}$, and both a rising σ_{v} and a velocity shear at still larger radii. Together, the observational evidence suggests that the discovered extended Carina population represents tidal debris from the dSph. Of 65 giant candidates at large angular radii from the Carina center for which MIKE spectra have been obtained 94% are associated either with Carina or a second, newly discovered diffuse, but strongly radial velocity-coherent (σ_{v}=9.8 km s^{-1}), foreground halo system. The fifteen stars in this second, retrograde velocity population have (1) a mean metallicity ~ 1 dex higher than that of Carina, and (2) colors and magnitudes consistent with the red clump of the Large Magellanic Cloud (LMC). Additional spectroscopy of giant star candidates in fields linking Carina and the LMC show a smooth velocity gradient between the LMC and the retrograde Carina moving group. We conclude that we have found Magellanic stars almost twice as far (22°) from the LMC center than previously known.

Subject headings: Carina Dwarf – galaxies: Local Group – kinematics and dynamics – Magellanic Clouds –cosmology : dark matter

1. INTRODUCTION

Whether the Milky Way dwarf spheroidal (dSph) satellite galaxies are undergoing tidal disruption remains a controversial question. Such tidal disruption would naturally lead to extended populations of stars that have been stripped from the satellite core. That *most* of the Milky Way (MW) dwarf spheroidals exhibit radial density profiles with extended components was suggested by the large area photographic survey of most of the Galactic dSph satellites by Irwin & Hatzidimitriou (1995, hereafter IH95). A number of studies have addressed the question of the reality of extended structural components around individual dSph examples — among them the Carina dSph, for which the issue has prompted lively debate (Kuhn et al. 1996, Majewski et al. 2000b, hereafter Paper II, Morrison et al. 2001, Walcher et al. 2003, Monelli et al. 2004). In a recent review of past and new work on the Carina system, Majewski et al. (2005, hereafter Paper VI) attempted to resolve the previous, apparently discordant results regarding the photometric detection of an extended Carina structural component. Paper VI showed that of all previous photometric surveys of Carina, that of Paper II — which makes use of the *DDO*51+Washington M, T_2 filter technique to identify giant stars (Majewski et al. 2000a, hereafter Paper I) at the distance of the Carina system — achieves the highest, and therefore most reliable, signal-to-background contrast in the diffuse outer parts of the Carina system. Moreover an extended, power-law component detected around Carina in Paper II is supported by spectroscopic confirmation of Carina giant candidates to 1.4 times the nominal limiting radius (r_{lim}) of the central-fitted King profile in Paper VI. Our previous work has therefore established the likely reality of the "King + power law" density profile for the Carina dSph.

In this paper (§3) we take advantage of a similar, but deeper and much wider area, photometric database of Carina than that presented in Paper II and, in addition, contribute higher-quality radial velocities (RVs) of Carina stars from echelle spectroscopy of giant star candidates to more than three times the angular separation from the Carina center than we explored in Paper VI. Carina-associated stars are now established to $4.5r_{lim}$ from the Carina core, leaving no doubt as to the reality of an extended component to the Carina system and imposing extreme limits on the mass of Carina if these stars are bound to the dSph (§4.6). To further improve the kinematical mapping of the Carina system at smaller radii, we also take advantage of archived, publicly available VLT+GIRAFFE spectra of more than 1000 stars near the center of Carina, which contribute more than 300 additional RVs

[1] Dept. of Astronomy, University of Virginia, Charlottesville, VA 22903-0818 (rrm8f, srm4n, pmf8b, ricky, dln5q@virginia.edu)
[2] Osservatorio Astronomico di Trieste, Via G. B. Tiepolo 11, I-34131 Trieste, Italy (zaggia@oats.inaf.it)
[3] Las Campanas Observatory, Casilla 601, La Serena, Chile (kunkel@jeito.lco.cl)
[4] Visiting Astronomer, Cerro Tololo InterAmerican Observatory, National Optical Astronomy Observatories
[5] Department of Astronomy, Wesleyan University, Middletown, CT (kvj@urania.astro.wesleyan.edu)
[6] Carnegie Observatories, 813 Santa Barbara Street, Pasadena, CA 91101 (crane@ociw.edu,shectman@ociw.edu)
[7] Korea Astronomy and Space Science Institute, 61-1 Hwaam-Dong, Yuseong-Gu, Daejeon 305-348 Korea (tonysohn@kasi.re.kr)
[8] Dept. of Astronomy, University of Michigan, Ann Arbor, MI 48109 (rabernst@umich.edu)

of Carina-related stars within the King limiting radius. The resulting velocity dispersion profile of the Carina system is the most extensive yet determined for any dSph galaxy, yet shows a continuation to large radii of the same more or less flat trend found (to smaller radii) in other Galactic dSphs (Muñoz et al. 2005; Westfall et al. 2006; Walker et al. 2005; Sohn et al. 2006) .

The present photometric and spectroscopic database of stars in the direction of Carina has yielded the additional discovery of a second apparently coherent stellar population in the foreground of the dSph (§6). This other Milky Way substructure is as dynamically cold as the Carina system itself and, ironically, represents the primary source of contamination within our previous (Paper II) and present photometric samples of Carina stars outside r_{lim}. The fifteen stars in our MIKE sample that are part of this other substructure share a number of properties (color-magnitude diagram position, metallicity, and velocity-angular separation trend) with stars of the Large Magellanic Cloud (LMC), but stretch some 22° from the LMC center. As with Carina, these widely separated stars place new, very large lower limits on the LMC mass and tidal radius if the stars are bound to their parent satellite.

2. NEW PHOTOMETRIC SURVEY

2.1. *Imaging Data*

Through spectroscopic follow-up of stars in the Paper II Carina database, Paper VI demonstrated the efficacy of Washington $M, T_2 + DDO51$ photometry to produce high quality candidate lists of giant stars from the Carina system to large separations from the core, and dispelled concerns (Morrison et al. 2001; Mayer et al. 2002; Walcher et al. 2003) that there may have been problems with the original methods or findings of Paper II. Nevertheless, a deeper, more uniform, and larger area $M, T_2 + DDO51$ survey of the Carina system was desired: Paper VI (see §2.4 of that paper) showed how the results of a survey with better photometry would improve the Carina giant candidate selection, whereas surveying to a larger angular radius would give greater insight into the extent and character of this outer Carina population.

Thus, new Carina photometry over a 10.74 deg^2 area (9.3 times more area than covered in Paper II — the area outlined below in Fig. 1) centered on the Carina dSph was obtained with the Mosaic wide-field imaging camera on the Blanco telescope on UT 2000 Feb 24-27 under photometric conditions. DAOPHOT II/ALLSTAR (Stetson 1987) PSF-fitting photometry was derived for stars in each of the individual Mosaic pointings, producing magnitudes with median errors of $(\sigma_M, \sigma_{T_2}, \sigma_{DDO51})$ = (0.018, 0.020, 0.015) at M = 20.8, which is approximately 3.4 mag below the Carina red giant branch (RGB) tip (Fig. 2). The photometry of this new survey is about 2 times more precise at that magnitude than the Carina data presented in Paper II. Instrumental magnitudes were calibrated into the standard system via multiple observations of Washington+*DDO*51 standards in Geisler (1996). Each star in our catalog has been corrected for reddening based on its Galactic coordinates by using the reddening map constructed by Schlegel et al. (1998). We found an $E(B-V)$ range of 0.033–0.102 in our Carina fields.

2.2. *Carina dSph Candidate Selection and Density Profile*

As in Paper II, the dereddened $(M-T_2, M-DDO51)$ two-color diagram (2CD) and the $(M-T_2, M)$ color-magnitude diagram (CMD) are used together to select stars most likely to be Carina giant stars. Figure 3 illustrates the selection criteria we used to identify Carina RGB stars: "Carina giant star candidates" are expected to fall primarily within the regions bounded by the solid lines in each of the diagrams in Figure 3. Because we want to create the most reliable maps of Carina density possible and because we choose to reserve the valuable Magellan echelle spectroscopic follow-up (§3) observing for the very best photometrically-selected candidates, our initial selection criteria were deliberately conservative. For example, we did *not* employ the proposed wider CMD selection criteria discussed in §3.2 of Paper VI, but maintained the more restrictive limits used in Paper II. In addition, our 2CD giant selection boundary is set far from the dwarf star locus to minimize photometric contamination (Fig. 3b) of the giant sample. However, the extensive, archived VLT+GIRAFFE spectroscopic data set for the Carina field, obtained for dSph candidates selected independently of our photometry and methodology, allows us in the velocity analysis described later (§4) to search for additional Carina stars with measured RVs that, while being excluded from our conservatively made "best" candidate lists, still occupy "RGB-like" regions of the CMD and 2CD (§4.1.3).

Across our survey area, the photometric sample is expected to be complete to M = 20.8, so we analyze the spatial distribution of giant candidates to this magnitude limit. In addition, because our spectroscopic survey is almost complete outside the Carina r_{lim} to T_2 = 18.4, we also analyze the spatial distribution of giants using this magnitude limit. Figure 4 presents the radial density profile derived for the Carina dSph for these two adopted magnitude limits. To create this profile, stars have been binned into elliptically-shaped annuli matching the Carina center, ellipticity and position angle found by IH95.

As discussed at length in Paper VI and Westfall et al. (2006), proper assessment of the background level (i.e. density of false positive detections) is critical to deriving dSph radial density profiles. Here we adopt two strategies for assessing this backgound level. In the case of the T_2-limited density profile, we can very accurately estimate the background directly from the results of our spectroscopic survey (§4), which is 90% complete for stars beyond the IH95 Carina r_{lim}. This spectroscopically-verified, true background[9] of 2.3 deg^{-2} within our "Carina giant candidate" star sample is subtracted from the observed density distribution of $T_2 \leq 18.4$ Carina dSph giant candidates across the entire survey to reveal the density profile shown in Figure 4a. Because of our near spectroscopic completeness for these stars, the density profile shown in Figure 4a beyond the IH95 r_{lim} virtually reflects the exact distribution of all RV-verified members there.

For our $M \leq 20.8$ sample, the background is estimated using the "CMD-shifting" method used in Paper II to estimate a background rate, with the one important difference that with our new survey here we are able to make exclusive use of the vast area outside of the Carina King limiting radius to significantly reduce potential contribution of any Carina stars not lying on the Carina RGB (e.g., asymptotic and post-asymptotic giant branch stars) that may have artificially inflated the estimated backgrounds in the Paper II execution of this method. On the other hand, we acknowledge that this method may also underestimate the contribution of the newly discovered halo substructure discussed in §6, since it has a similar CMD position as the Carina dSph. To correct for this, we add back

[9] This is the background level scaled to a 100% spectroscopic completeness level.

into our background estimate the fractional contribution of stars from this substructure among the spectroscopic sample of $> r_{lim}$ stars chosen as Carina giant candidates. This yields a conservative[10] background level of 10.3 deg^{-2}, which is then subtracted from the observed density distribution of $M \leq 20.8$ Carina RGB candidates.

The two samples with the two methods of background calculation produce remarkably consistent radial profiles (Fig. 4). In both cases, the central part of the density profile is well described by the normalized IH95 King profile (shown by the solid line) for Carina, which is characterized by r_{lim} = 28.8 arcmin and a core radius of 8.8 arcmin. Both radial distributions also show a prominent, second "break population" roughly following a power-law decline to the limits of our present survey. The dashed lines correspond to power-law indices of -1.5, -2 and -2.5 respectively. A -2 index power law appears to yield a reasonable match to the density fall-off of the break population, although power laws with indices of -1.5 or -2.5 cannot be discounted; in general, the power law here is steeper than found in Paper II, owing to a slightly higher background derived in this study (see also a discussion of this steeper slope in Paper VI). Nevertheless, in this completely new photometric survey with substantial spectroscopic follow-up we have independently borne out the general conclusion of Paper II and Paper VI that Carina exhibits a prominent, extended, power-law break population.

As discussed in Paper II, the density profile exhibited in Figure 4 mimics that of model disrupting dSph galaxies (see, e.g., Fig. 15 of Johnston et al. 1999). With our updated version of the Carina density profile, we can revisit the implied fractional mass loss rate according to the method of Johnston et al. (1999) under the assumption that the power law population represents unbound tidal debris. We derive a fractional mass loss rate for Carina of $(df/dt)_1$=0.075 Gyr^{-1}, but we must note that this method is technically derived for break populations following a -1 power law, and even in that case it only yields estimates good to within a factor of two. Perhaps a better estimate of the fractional mass loss rate comes from the $(df/dt)_2$ method of Johnston et al. (1999) using the corrections given by Johnston et al. (2002); this method yields un upper limit for the Carina mass loss rate of $(df/dt)_2 < 0.24$ Gyr^{-1}. In a subsequent paper (Muñoz et al., in preparation, hereafter M06) we use this newly derived density profile as well as the velocity dispersion profile derived in §4.3 to model the mass loss history using N-body simulations specific to the Carina dSph, and derive likely mass loss rates generally between these two estimates.

3. SPECTROSCOPIC DATA

3.1. *Spectroscopy with MIKE*

The Carina power-law population has been of particular, though not exclusive, interest during our follow-up spectroscopic observations. Paper VI presented radial velocity observations obtained with the Blanco telescope + Hydra multifiber system. Only some of these observations were of sufficient resolution to contribute reliable information on the internal dynamics of (rather than simply stellar membership in) the Carina dSph. Thus, on UT 2004 Jan 27-28 and Dec 29-30 good spectra of a total of 77 Carina giant star candidates selected from the new photometric survey were obtained using the Magellan Inamori Kyocera Echelle (MIKE) spectrograph on the Clay 6.5-m telescope at Las Campanas; this instrument delivers $R \sim 19000$ resolution spectra over the red echelle orders we used for this work. Of the 77 stars targeted, 65 were selected to be giant candidates by the giant selection shown by the solid lines in Figure 3 and 12 were selected using an expanded 2CD selection (shown by the dotted lines in the same figure). This wider 2CD giant selection corresponds to that derived in Paper I. More than half (40) of the 77 stars observed with MIKE lie outside the nominal Carina r_{lim} as determined by IH95; the rest are scattered throughout the region inside the King limiting radius, but primarily at larger radii where few previous Carina spectra have been obtained.

Radial velocities (RVs) have been derived via cross-correlation of the MIKE spectra against a "universal template" containing sets of stellar atmospheric absorption lines that typically give the strongest correlations to the spectra of late type stars; apart from these lines, the bulk of the spectra and templates are masked out because these wavelengths contribute more noise than signal to the cross-correlation spectrum. Prior to cross-correlation, the spectra are also Fourier-filtered to remove irrelevant low frequency features as well as features with higher frequency than the intrinsic resolution of the spectrograph. A fuller discussion of this cross-correlation technique is given in Majewski et al. (2004a); but we have found that the procedure works just as well, or even better, for $R = 19,000$ spectra than for the moderate resolution spectra cross-correlated in that paper. We observed to high S/N a number of K giant velocity standard stars that we used to measure small systematic offsets imposed on the derived RVs that are particular to the nature of the adopted artificial template. Our cross-correlations here were conducted over the echelle order (spanning 8468-8693 Å) that contains the calcium infrared triplet and over a dozen other useful lines in stars as metal poor as Carina ([Fe/H] ~ -2). Tests with other, nearby orders yield similar RV results but of lower reliability, so the values given here are based solely on the calcium triplet order, where the typical S/N of the stellar continua were 7-12 per pixel. This particular echelle order also contains ample numbers of telluric absorption features with strengths great enough to yield useful velocities. Since the stars were observed with a 0.9 arcsec slit whereas the seeing often was as good as 0.7 arcsec, significant fractional errors in derived RVs may arise from slit centering errors. To measure the velocity shifts that result from this effect, we independently cross-correlate the telluric absorption features in each order against those in a set of observed RV standards as well as in dusk spectra (see discussion in Sohn et al. 2006). These RV standards were typically exposed by smoothly passing them across the slit during the integration to create a symmetric net slit function for the resulting spectra. By comparison of multiple spectra obtained of several Carina giants as well as by comparison of results from cross-correlation of different echelle orders, we find the random errors in the derived RVs to be better than 1.0 km s^{-1} for the January run and 2.5 km s^{-1} for the December run. The degradation in the second run was due to significantly worse overall observing conditions that resulted in poorer S/N spectra on average.

Table 1 gives for the stars observed with MIKE the J2000.0 positions, date of spectroscopic observation, photometric data, RVs in both the heliocentric and Galactic standard of rest (v_{GSR}) conventions, as well as a parameter that characterizes the quality of the RV: an overall quality index, Q, which ranges from 1 (lowest quality) to 7 (highest quality).

[10] The procedure just described *ignores* the fact that much of the §6 substructure is actually *outside* our CMD selection criterion, to make the most generous estimate of the background.

The precise meaning of the various Q grades is explained in Kunkel et al. (1997a) and Majewski et al. (2004a).

As an additional check on the RVs, we independently derived RVs for all MIKE spectra using the `fxcor` package from IRAF[11] following the method described in Frinchaboy et al. (2006). The mean RV difference between both methods is 0.1 ± 0.4 km s^{-1} with a dispersion of 2.8 ± 0.3 km s^{-1} showing a very close correspondence between the methods. However, for some spectra with very low S/N our standard methodology failed to yield an acceptable (i.e. $Q \geq 4$) cross-correlation, whereas `fxcor` yielded a cross-correlation with higher apparent reliability. In these cases we have adopted the fxcor RV in Table 1 and given the derived velocity error in place of the Q value.

In the end, all 65 Carina-giant candidates observed with MIKE have a reliable velocity and these form the basis of most of the outer Carina RV analyses below. Among the 12 stars with RVs selected from the expanded giant selection criterion in Figure 3b, none have been found to have a Carina-like velocity; however, two of these stars have velocites near $v_{hel} \sim 332$ km s^{-1} and constitute members of the newly discovered halo substructure discussed in §6. Thus we include these two stars in our discussions relevant to this halo substructure.

3.2. *The GIRAFFE Spectra*

Because our MIKE observing focused primarily on the most widely separated Carina giant candidates, our resulting spectroscopic coverage leaves a significant statistical gap from the only other previously published echelle resolution Carina RVs, which are in the Carina core (Mateo et al. 1993). Fortunately, there exists a substantial collection of archived VLT/FLAMES observations of the Carina system that bridges the gap.[12] These data were retrieved and reduced to RVs by S.Z. and D.C..

FLAMES is installed at the Nasmyth A focus of the VLT Kueyen telescope and is composed of a fiber positioner, OzPoz, that feeds the dedicated medium-high resolution GIRAFFE (resolving power $R \simeq 6000-30000$) and UVES ($R \sim 40000$) spectrographs with 132 and 8 science fibers, respectively, over a large field of view ($\simeq 28$ arcmin in diameter) in the "MEDUSA" mode. The VLT Carina data set used in this paper was collected over a 9 night run at the end of 2003 (22-31 December) and consists of 16 different pointings, each observed four times. The exposure time was 4×3300 seconds per pointing. The four exposures for each pointing were taken in sequence and with the same MEDUSA plate configuration. All observations were done using GIRAFFE in the low resolution, LR08 set-up having $R \simeq 6500$, and centered on the Calcium infrared triplet to cover the region from 8206 to 9400 Å . At the end of each observing night, during daylight, a sample of calibration frames were taken by the VLT staff within the nominal VLT calibration plan.

Spectroscopic calibration and extraction have been performed with the GIRAFFE BLDRS[13] data reduction pipeline (version 1.12) and the GIRCALIB calibration reference file database (version 2.3). The GIRCALIB image database contains generic reference solutions for the calibration frames (bias and dark frames, flat-fields, fiber slit geometry and fiber response correction frames as well as wavelength calibration for all the different FLAMES observing modes) that are used as initial guesses for specific night-to-night solutions for all the different calibration steps. For each night, the calibration frames (bias, flats, wavelength calibrations) are grouped together and reduced with the appropriate recipe, starting with the reference solution in the GIRCALIB database and then iterating corrections to it. Once all of the solutions are found they are applied with a single command to the science images.

No particular problems were encountered in the reduction of the calibration frames, but occasionally the wavelength calibration gave unstable and distorted solutions due to the uneven spacing and scarce number of ThAr calibration lines in the available spectral range. To overcome and check this problem, for each wavelength calibration frame used (one per night taken during the daytime) the emission line detection threshold and fitted polynomial order were readjusted until a satisfactory solution was obtained. These solutions were then verified directly by the ThAr-calibrated science spectra (before night sky subtraction), which were cross-correlated with a separate, emission line night sky spectrum calibrated externally with the detailed night sky line lists of Osterbrock et al. (1996, 1997). It was found that the average RMS velocity scatter from fiber to fiber based on the sky-lines was an acceptable 0.87 km s^{-1}. We adopt this value as our wavelength zero point error for the GIRAFFE spectra. The same test revealed that the offset from plate to plate was less than 0.2 km/s; nevertheless, we corrected all plates to the same radial velocity zero point system based on the night sky lines.

The archived GIRAFFE images contain spectra from all of the fibers for a given MEDUSA plate. Between 109 and 112 MEDUSA fibers were placed on target stars depending on the pointing, with the remaining fibers positioned on empty sky positions. The identification of the target objects associated with each spectra is possible using associated archived tables containing the observers' input values of target positions and magnitudes as well as details of the positioning of the fiber on the sky.

Radial velocity derivations were performed using an implementation of the Tonry and Davis (1979) method in the MIDAS environment. We extracted radial velocities both for each single exposure of each medusa plate and then for the sum of the four exposures per plate. For each exposure we first extracted the sky fibers to create a sky spectrum for that exposure. This sky spectrum was subtracted from each target fiber spectrum and the result was continuum-normalized and finally cross-correlated with a synthetic spectrum[14] of a low metallicity giant star to obtain the radial velocity. In the second reduction method we summed the four extracted and sky-subtracted spectra for each star and cross-correlated *that* with the template spectrum. The comparison of the single spectra and the summed spectra RVs for each object revealed that the RVs from the former were very poor, especially for the faintest stars: several times we failed completely to measure a reliable RV. In the cases where we were able to get four in-

[11] IRAF is distributed by the National Optical Astronomy Observatories, which are operated by the Association of Universities for Research in Astronomy, Inc., under cooperative agreement with the National Science Foundation.

[12] The archived FLAMES/VLT data set used in this paper is part of the ESO large program 171.B-0520 "Towards the Temperature of Cold Dark Matter: Quantitative Stellar Kinematics in dSph Galaxies", PI. G. Gilmore.

[13] The GIRAFFE BLDRS, Base Line Data Reduction Software, is a set of python scripts, modules and a C library to reduce GIRAFFE spectra. The software and documentation can be found at http://girbldrs.sourceforge.net/.

[14] We built the template spectrum using the Kurucz models properly simulated for the GIRAFFE spectrum resolution and set-up used. We tested several templates and finally adopted a spectrum for a star with T_{eff} = 4500, log$g$ = 2.5 and [Fe/H]= –1.5.

dependent RVs we compared their average with the RV of the summed spectrum and found that the RMS was much larger than the measurement error in 80% of the sample. Thus, we decided to use only the RVs derived from the summed spectra.

A total of 1771 independent radial velocity measurements were obtained across the sixteen medusa pointings. After removing 66 stars for which we could not get an RV and accounting for repeated targeting of some stars, RVs were obtained for 994 distinct stars. In the final definition of the RVs we found that among objects having more than three measurements ($\simeq$ 130 stars) the scatter was always compatible with the measurements errors except for the very faintest objects where we found a larger scatter. The RV errors take into account this larger scatter. Of the 994 individual GIRAFFE target stars, 975 were found in our Washington+*DDO*51 photometric catalog. We only consider those 975 in our analysis because the remaining 19 stars not present in our photometric catalogues cannot be checked for their giant status in the 2CD.[15] Table 2 presents the RV information for these stars.

To the MIKE and GIRAFFE data we also add Blanco+Hydra RVs for photometrically selected giant stars from Paper VI that were observed at $R = 7600$ resolution in October 2001. We include these Hydra RVs only for those stars not already having higher resolution echelle observations. In the end, our sample includes a total of 1123 RVs from Table 1, Table 2, Mateo et al. 1993 and the Paper VI contribution.

4. SPATIAL AND RADIAL VELOCITY DISTRIBUTIONS OF CARINA DSPH MEMBERS

4.1. *Definition of Carina dSph Members*

4.1.1. *The Full Sample*

Figure 5a shows the distribution of all derived RVs for stars in the Carina field as a function of elliptical distance from the center, including stars having RVs from Mateo et al. (1993) (green points), Hydra observed stars from Paper VI (cyan points), stars with MIKE RVs (red points), and GIRAFFE data (blue points). The elliptical radius of a star is defined to be the semi-major axis radius of the ellipse centered on Carina (with the ellipticity, center and position angle for the dSph as found by IH95) that passes through the star. Figure 6a shows the integral of the RV distribution over all radius. A most obvious characteristic of these "full sample" RV distributions is the presence of the prominent RV peak associated with the Carina core near $v_{hel} \sim 220$ km s^{-1}. However, a significant contribution of stars at other RVs may be seen, particularly from stars with $v_{hel} \lesssim 150$ km s^{-1} from the Milky Way. These contaminants come predominantly from the GIRAFFE sample, which was apparently primarily selected on the basis of positions of stars in the CMD. While the Carina RV peak still stands out, the substantial background of non-Carina stars makes it difficult to define an accurate RV criterion for cleanly isolating Carina members.

4.1.2. *The Conservative Sample*

Figures 5b and 6b show the same RV distribution, but only for stars satisfying the conservative Figure 3 criteria for identifying Carina giant candidates by their Washington $M, T_2 + DDO51$ photometry. This distribution of the "best" photometric candidates makes it easier to define an appropriate additional criterion, based on RVs, for identifying Carina members. Anticipating that the velocity dispersion of Carina members actually rises slightly outside the Carina core, we define as an RV membership criterion the 3σ range defined by RVs for Carina stars beyond $r_e > 0.6 r_{lim}$ (twice the core radius), where we find a mean $v_{hel} = 220.8 \pm 1.3$ and a $\sigma = 10.2$ km s^{-1}.[16] This range is indicated by the dashed lines in Figure 5b and the shaded region in Figure 6b. This new RV selection criterion for MIKE and GIRAFFE stars is narrower than that applied in Paper VI, but this is because the RVs in the present sample have smaller random errors. This final set of stars, selected by our conservative CMD and 2CD criteria (Fig. 3) is shown in Fig. 5b.

An additional feature apparent within the RV distribution of the "best photometric sample" in Figure 5b and 6b is the distinct group of stars with a clumped RV at an even *more* extreme velocity than the Carina dSph. This feature is even more clear in Figure 6d, where we show a histogram for a subsample of stars from Figure 6b, in particular, stars with $r_e > 1.5 r_{lim}$. Their $v_{hel} \sim 332$ km s^{-1} implies a significant retrograde motion for stars in this direction of the sky. The magnitudes and colors of these stars (Table 1) are also rather clumped, indicating similar spectral characteristics and an apparently similar (and substantial) distance. In §6 we explore further this moving group of giant stars from what appears to be a newly found halo substructure.

4.1.3. *Expanding the Conservative Sample*

A comparison of Figures 5a and 6a with Figures 5b and 6b suggests that the restrictiveness of our "conservative" photometric selection of Carina giants, while providing extremely pure samples of Carina stars, also leads to a non-negligible level of incompleteness (a well-known issue we have addressed before in §3.2 of Paper VI). Given that we now have the advantage of three criteria for discriminating Carina giants and a large number of RVs from GIRAFFE in the Carina main body, it is worth reinvestigating the tradeoffs between sample size/completeness and sample purity. More specifically, can we expand any of the selection limits to admit substantially more Carina stars from the GIRAFFE sample without sacrificing the reliability of the membership census.

2CD outliers: Figure 7 demonstrates some possibilities for expanding our membership acceptance criteria by showing the 2CD and CMD of stars satisfying our newly established Carina RV-membership criterion, but falling outside one or the other (or both) our conservative photometric criteria (plotted as the solid lines in Figs. 3 and 7). As may be seen in Figure 7b, a large fraction of these stars lie *just below* our Figure 3b giant selection in the 2CD. However, inspection of the distribution of stars in Figure 3b clearly shows a strong, almost vertical giant star 2CD concentration at $(M - T_2)_0 \sim 1.2$ that extends below the adopted diagonal limit there. Moreover, the 2CD analysis of giant and dwarf stars presented in Paper I makes clear that giant stars are commonly found at these positions of the CMD — a point demonstrated by the superposition of the Paper I "giant star boundary" in Figure 7b (dotted lines). Stars in Figure 7 lying within the Paper I 2CD boundary but within the Figure 3a CMD boundary are

[15] The 19 stars missing from our catalogue are primarily due to the loss of stars in the gaps between CCD chips in our Mosaic images as well as to small gaps in the placement of our Mosaic pointings within r_{lim}, visible in Figure 1. We note that only 10 of these 19 stars have RVs consistent with the Carina dSph.

[16] The velocity dispersions shown later in Fig. 11 are at lower values than the observed spreads in Fig. 5 because the former have been corrected for measurement errors.

marked with red open triangles in Figure 7. Given that these stars satisfy the RV, CMD and the Paper I 2CD criteria, we regard these stars as Carina giants from here on.

CMD outliers: We may also investigate those stars that satisfy the RV and 2CD criteria but not our initial CMD boundary. In Figure 7 these stars are marked with open blue circles for the stars that satisfy the stricter of the 2CD boundaries and green open circles for the stars satisfying the Paper I 2CD limit. Almost all of these lie very close to the RGB limit. A number of them lie at a CMD position just above the strong red clump. Given that Carina has stellar populations as young as 0.6-1.0 Gyr (Monelli et al. 2003), it might not be too surprising to find some core He-burning stars lying above the canonical red clump from the dominant, older, more metal-poor Carina population (e.g. Salaris & Girardi 2002). Other modest CMD outliers are in CMD positions consistent with those expected for asymptotic giant branch stars. A similar outlier trend was found in Paper VI, where it was noted that slightly expanding the magnitude width of the CMD selection criterion by a few tenths of a magnitude would increase completeness with virtually no decrease in reliability. Given that previous conclusion, and that these stars satisfy the 2CD and RV criteria, we consider all of these outliers as Carina members.

RV outliers: Finally, what about stars that fall within the 2CD and CMD criteria but just outside the RV criterion? Several of these stars are conspicuous in Figure 5b. First, we note that there are ~ 300 stars satisfying our 3σ RV criterion in Figure 5b. For a sample of this size and with a Gaussian distribution, one expects $\sim 0.3\%$, or ~ 1 outlier. As may be seen in Figure 5b, two stars with $r_e/r_{lim} < 0.6$ lie just below the RV cutoff and are probably very likely this kind of Gaussian-wing outlier member. These stars (C2661 and C161179) are indicated by the blue solid squares symbols in Figures 5 and 7, where they can be seen to be very solidly photometric members. Nevertheless, because they are in the well-populated central part of Carina, whether or not they are included in our analyses has very little effect.

On the other hand, as we discuss in §4.5, the velocity dispersion of Carina appears to grow beyond the King limiting radius, and, even though our RV selection criterion was derived from stars with $r_e/r_{lim} > 0.6$ specifically for this reason, the RV dispersion that sets the selection criterion is dominated by stars with $0.6 < r_e/r_{lim} < 1.5$. Beyond this range, the dispersion not only grows, but, as we show in §5, the RV distribution becomes flatter than Gaussian. Both larger velocity dispersions as well as more platykurtic velocity distributions are fully consistent with models of disrupting dSphs systems (Read et al. 2005a; M06). Thus, even wider separated RV-outliers are not only conceivable at large radii, they are expected. We mark three of these from our MIKE sample — C1960448, C2450090 and C2050415 — with red square symbols in Figures 5b and 7. These stars, which lie within ~ 28 km s^{-1} (3σ), ~ 20 km s^{-1} (2σ) and ~ 10 km s^{-1} (1σ), respectively, of our Carina RV membership limit, are again solidly within the photometric Carina giant candidate selection criteria (Figure 7). They are particularly interesting potential members, since all three lie approximately along the Carina major axis, and at large radii — ~ 2.0 deg to the east, ~ 1.6 deg southwest and ~ 2.0 deg northeast of Carina center, respectively (see Fig. 8a). Indeed, the latter star is potentially the most widely separated Carina giant in our sample, at $r_e = 4.9 r_{lim}$.

Nevertheless, unlike in the cases of the sample-admitted 2CD and CMD outliers above, even though we can make a compelling case for the membership of all five of these RV outliers, we *exclude them* from our dynamical analyses to follow, so that we do not unduly bias our velocity results. Figures 5c and 6c summarize the RV distributions of our final, expanded Carina-member sample based on our two (slightly widened) photometric criteria and one velocity criterion. In Tables 1 and 2 we designate by the column "Member" those 260 stars considered to be members by the most conservative criteria and those additional 116 stars that have been admitted as Carina members by the exceptions described in this subsection. We stress that (1) all 116 of these stars are from the GIRAFFE sample, (2) all but 2 are within $r_e < 0.9 r_{lim}$ and so have no impact on the dynamical results at larger radii, and (3) the inclusion or exclusion of these 116 stars in our analysis has little effect on the general dispersion trends described later (Fig. 11). Thus we have opted to include these 116 stars to improve our sampling and statistical uncertainties. The five RV outliers discussed above but not included in our analyses are highlighted in this column by "RV?".

4.2. *Sky Distribution of Carina dSph Members*

The azimuthal distribution of the Carina RV-members on the sky (Fig. 8a) shows them to lie predominantly along the Carina major axis, even though, as shown in Figure 1, the azimuthal coverage of our photometric and spectroscopic efforts actually favors the *minor* axes (see, e.g., the distribution of Carina giant candidates *not* found to be RV members in Fig. 8b). Figure 9, which shows the ratio of the circular to elliptical radius (r_c/r_e) for each star in the survey versus its circular radius, demonstrates the tendency for Carina RV members outside the King limiting radius to lie along an extension of the position angle of Carina's ellipticity and, indeed, to have an apparently even more elliptical distribution in this direction at larger radii. Stars on the major axis will have $r_c/r_e = 1$ and stars on the minor axis will have $r_c/r_e = 0.67$, according to the ellipticity of Carina (IH95). That the mean r_c/r_e increases at larger r_c shows the tendency for the extended population to become even more stretched along the major axis, evokes the character expected of tidal tails, and is a key characteristic of dSph tidal disruption models (Oh et al. 1995; Piatek & Pryor 1995; Johnston et al. 2002; Choi et al. 2002; M06). Further surveying for Carina members over larger radii to see whether and how this trend may continue would provide a valuable check and important constraint on the nature of any tidal disruption.

4.3. *Photometric Contamination Levels Revisited*

Paper VI has already focused on the reliability of our methodology to assess dSph structure into extremely low surface brightness regimes, with specific focus on Carina. However, with the now much better spectroscopic coverage as well as better photometry of the Carina field we may reassess the effectiveness of our Washington $M, T_2, DDO51$ survey strategy. In addition, the MIKE spectroscopic sample, which was pre-selected based on the Washington+DDO51 photometry, provides an interesting contrast with the GIRAFFE sample, which was not.

A straight calculation of our success rate from the 48 Carina RV-members among all 65 Carina giant candidates with MIKE spectroscopy yields a success rate of 74% in identifying true dSph members. Restricting the analysis to only stars outside the nominal (IH95) King limiting radius yields a success rate of 55% (22 dSph members among 40 $r_e > r_{lim}$ Ca-

rina giant candidates with RVs), and this includes candidates at extremely low densities (0.058% the density of the Carina core). However, 13 of the 40 Carina giant candidates outside r_{lim} with determined RVs appear to be giant stars from *another* tidal stream with rather similar CMD characteristics as Carina (§6). Though these stars are not attributable to Carina, this newly discovered Milky Way feature might be argued as a success of the overall methodology we have been using in this series of papers to identify just this kind of halo substructure. Were we to combine these stars with the true Carina dSph members, our success rate in identifying "halo substructure" stars rises to 94%.

In contrast, the original GIRAFFE sample was apparently selected only on the basis of the position of these stars in the CMD (though not our CMD). Among the 975 stars in the GIRAFFE sample also in our catalogue, 390, or 40.0%, are found to have Carina RVs — and this is for a sample highly concentrated to the main body of Carina, with most stars having $r_e < 1.0 r_{lim}$. However, had we applied our photometric selection criteria to the GIRAFFE catalog 97.3% of the stars identified as Carina giant candidates would have been found to be RV-members (almost tripling the telescope efficiency). Combining all available RV data at all radii, the Washington+DDO51 pre-selection results in a 90.5% RV-member efficiency. Thus, the combination of Washington+*DDO*51 photometry with quality spectroscopy is found once again (see Palma et al. 2003, Westfall et al. 2006, Sohn et al. 2006) to be a very effective observational strategy for identifying very diffuse halo substructures.

The point is relevant to potential further work on the extended structure of the Carina system. Continued searches for Carina giants at large separations from the dSph center will require an efficient means to identify the best candidates to optimally take advantage of spectroscopic time on the largest telescopes. We note that using *only* a selection for Carina stars by their position along the Carina RGB in the CMD becomes a very inefficient way to find Carina giants at $3r_{lim}$: At these radii, only one in 85 stars in the RGB selection region in the CMD we have used (Fig. 3b) turns out to be an actual Carina giant, and to $M = 20.8$, the density of such stars is only 7.4 deg^{-2}, making even multifiber spectroscopic searches for members within a CMD-only target list a rather inefficient enterprise.

4.4. *Standard Mass-to-Light Determination Revisited*

Estimates for the central and global Carina M/L determined using standard prescriptions (e.g., core-fitting combined with the central velocity dispersion) are given by Mateo et al. (1993) as $(M/L)_{\rm o} = 40 \pm 23$ and $(M/L)_{tot} = 37 \pm 20$ (all M/L values in solar units), respectively, when isotropic, single-component (King 1966) models are adopted; anisotropic models were argued to give similar global M/L for the lowest possible central mass density. These values were based on an observed central velocity dispersion of 6.8 ± 1.6 km s^{-1}. Monte Carlo analyses conducted Mateo et al. (1993) show that it is unlikely that this dispersion has been inflated by either atmospheric jitter in the target K giants or the influence of binaries.

However, there seems to be no real consensus on derived M/L's for Carina. For example, Mateo (1998) quotes the Carina $(M/L)_{tot}$ as 31, whereas IH95, adopting the original Mateo et al. (1993) central velocity dispersion, derive $(M/L)_{tot} = 59 \pm 47$ and $(M/L)_{\rm o} = 70 \pm 50$ (where the large error bars reflect uncertainties in the velocity dispersion, core radius and at least a factor of two uncertainty for the central surface brightness). Walcher et al. (2003) estimate the Carina mass and M/L by assuming that its periGalactic tidal radius can be approximated by r_{lim} (obtained from their photometric survey of the dSph) and using the Oh et al. (1992) relationship between the tidal radius of a satellite and its mass and orbit. Circular orbits yield M/L as low as 0.6 while more eccentric orbits can easily accommodate values as high as the ones derived by Mateo et al. (1993), but Walcher et al. (2003) derive a Carina $(M/L)_{best} = 17$ based on an orbit with eccentricity 0.6 and apoGalacticon twice that of Carina's current distance.

The new RV dataset presented here invites yet another M/L evaluation. Unlike previous determinations making use of a "central" velocity dispersion from a relatively small number of stars in the very core of the dSph, our extensive and radially continuous velocity coverage means that the definition of "central" is not pre-defined by our available sample. If we assume that at least the inner parts of the dSph are well represented by a King profile, Figure 4.11 from Binney & Tremaine (1987) shows that the velocity dispersion of stars begins to deviate from its central value at about half the core radius. Figure 10 shows the central velocity dispersion of Carina as we grow the radius (shown in units of core radius as measured by IH95) within which we include RVs in the dispersion computation. As we add successive stars out from the Carina center the derived "central" velocity dispersion (calculated using the maximum likelihood method, Pryor & Meylan 1993; Hargreaves et al. 1994; Kleyna et al. 2002) reaches a value of 6.97 ± 0.65 km s^{-1} at half the core radius (computed from 87 total Carina stars). This value, which is slightly larger than (but consistent with) the 6.8 km s^{-1} value used by Mateo et al. (1993), is adopted to rederive the Carina M/L's.

The central mass-to-light ratio can be determined as (Richstone & Tremaine 1986):

$$(M/L)_{\rm o} = \frac{\rho_{\rm o}}{I_{\rm o}} = \eta \frac{333\sigma_{\rm o}^2}{r_{1/2} S_{\rm o}} \quad (1)$$

where η is a correction parameter dependent on the concentration value (0.955 for Carina), $r_{1/2}$ is the geometrical mean of the half-light radii measured along the major and minor axis (163 ± 26 pc) and $S_{\rm o}$ is the central surface brightness (2.2 ± 1.0 L$_\odot$/pc^2). We adopt all these structural values from IH95[17] and obtain $(M/L)_{\rm o} = 43^{+53}_{-19}$ for Carina where the main source of uncertainty comes from the uncertainty in the central surface brightness. To illustrate this, we calculate the error in the $(M/L)_{\rm o}$ not considering the uncertainty in the central surface brightness, and obtain $(M/L)_{\rm o} = 43^{+8}_{-7}$.

From Illingworth (1976):

$$(M/L)_{\rm tot} = \frac{166.5 R_{c,g} \mu}{\beta L_{\rm tot,V}} \quad (2)$$

where $R_{c,g}$ is now the geometric-mean King core radius in pc (210 ± 30), μ is the King (1966) dimensionless mass parameter, and β is a model-dependent velocity parameter related to the observed velocity dispersion. Table 10 in IH95 gives values for both μ and $\sqrt{\beta\sigma_{\rm o}^2}$ of 2.8 ± 1.3 and 0.52, respectively, for a Carina concentration of $\log(r_t/r_c) = 0.52$. This yields $(M/L)_{\rm tot,V} = 41^{+40}_{-25}$ for a $L_{\rm tot,V} = 0.43 \times 10^6$ (Mateo 1998).

[17] Aside from fitting the presently derived Carina density distribution, these parameters also fit well the Carina distributions in Walcher et al. (2003) and Paper II. Moreover, they fit our data better than the parameters derived by Walcher et al. (2003) from the theoretical King model (King 1966).

This translates into a total mass of $M_{\rm tot} = 1.76^{+1.75}_{-1.10} \times 10^7$ M$_\odot$. These results are in very good agreement with the ones found by Mateo et al. (1993) despite the fact that the structural parameters they use are different from the IH95 ones adopted here. Here we adopt the updated distance of Carina from Mateo (1998), which is larger than the value used by Mateo et al. (1993), and this results in a larger half-light radius that compensates for the slightly larger luminosity adopted here.

4.5. *Velocity Dispersion Trend of Carina Stars*

With this large RV dataset in hand we can now assess the velocity dispersion behavior for Carina to well past r_{lim}. To ascertain this trend, we have studied the velocity dispersion as a function of both elliptical and circular angular distance from the Carina center. Because the true shape of the gravitational potential and tidal boundary of a dSph are likely to be somewhere in between these limiting shapes, it is helpful to explore these two limiting cases. In each calculation of an RV dispersion 3-σ outliers have been removed iteratively, with the mean velocity for each bin reevaluated at each iteration and the dispersions estimated using the maximum likelihood method. We note that this method assumes that the velocity distribution follows a Gaussian distribution everywhere which is not strictly true for Carina. However, such non-Gaussian behavior is apparent only in the outskirts of Carina ($r \gtrsim r_{lim}$; §5), and the effect of the non-Gaussian character found there is that the dispersion will tend to be slightly underestimated by the maximum likelihood method.

Figure 11 shows the derived Carina velocity dispersion profiles for both choices of angular separation: the left panels show profiles plotted against elliptical radius, the right shows the same for circular radius. To test binning effects, we have used both 23 and 46 stars per bin (lower and upper panels respectively) for stars inside r_{lim}, but because the number of stars with measured RV beyond this point is sparse, the last four dispersion points in each plot are binned at 10 stars each.

The Figure 11 Carina profiles remain fairly flat throughout the radial extent of the main body of the dSph, to $\sim 1.1 r_{lim}$. Such flat profiles over a comparable structural radial range have now been reported (although not to the radial extent of this study) for several dSphs: Sculptor (Tolstoy et al. 2004; Westfall et al. 2006), Draco (Muñoz et al. 2005), Ursa Minor (Muñoz et al. 2005), Fornax (Walker et al. 2005), Leo I (Sohn et al. 2006) and Sagittarius (Majewski et al., in preparation). Note that while Wilkinson et al. (2004) found a sudden drop in velocity dispersion at about r_{lim} for both Ursa Minor and Draco, this feature could not be reproduced by Muñoz et al. (2005) when reanalysing these profiles when Washington+*DDO*51 photometric and additional spectroscopic data were used to check them. Kleyna et al. (2004) have also found Sextans to have a predominantly flat profile but with a cold velocity dispersion at about r_{lim} (and a kinematically cold center as well); given that similar claims for cold points near r_{lim} in the Ursa Minor and Draco dSphs have not held up under further scrutiny, the Sextans result warrants further investigation.

Flat velocity dispersion profiles are incompatabile with mass-follows-light dSph models (with or without dark matter) in complete dynamical equilibrium, where decreasing dispersions are expected at large radius, approaching zero as the cutoff radius of the distribution is approached. To explain the observed velocity behavior, Walker et al. (2005) suggest that the *easiest* assumption to discard is that mass follows light; following this line of reasoning, a number of groups (e.g., Łokas et al. 2005; Xiao et al. 2005; Read et al. 2005b; Mashchenko et al. 2005b; Walker et al. 2005) have invoked "two-component dSph models", where the dark mass extends far beyond its luminous counterpart and is responsible for the flat dispersion profile at large radius. Yet, our MIKE observations of Carina have now yielded the most extensive coverage of velocities in any dSph, including, for the first time, the measurement of the velocity dispersion of a dSph (apart from Sgr) with a reasonable sample of stars beyond $2r_{lim}$. As may be seen in Figure 11, the velocity dispersion for Carina approximately doubles at these large separations — a result that is *not* explained with previous two-component models.

Is abandoning mass-follows-light really the "easiest" assumption to discard in the dSph models? Flat dispersion profiles arise *naturally* in tidal disruption models (Kuhn & Miller 1989; Kroupa 1997; Fleck & Kuhn 2003) *even if large amounts of dark matter are present* and the central parts of dSphs are bound and in equilibrium (Mayer et al. 2002; Sohn et al. 2006). As we show in M06, a single-component, mass-follows-light, tidally disrupting dSph model gives a good representation for both the density and velocity dispersion profile for the Carina dSph we have derived here.

Further evidence for a disruption scenario is provided by the trend of velocity across the satellite. In Figure 12 we show the mean RV (in Galactic Standard of Rest) as a function of *b*-distance from the center of Carina (approximately the major axis of the satellite). No significant RV trend in the central part of Carina that resembles a rotation curve is observed. However, beyond r_{lim}, a gentle velocity gradient is observed across the major axis of Carina to the extent of our observations. Over ~ 1.2 degree (2.1 kpc), a peak-to-peak difference of ~ 10 km s^{-1} is seen in this trend — a difference significantly larger than the error in the means for the binned points. This velocity trend is interesting because it has been predicted as a hallmark of tidal disruption by several studies (e.g., Piatek & Pryor 1995; Johnston et al. 1999, Fleck & Kuhn 2003). According to Pryor (1996), "a velocity gradient across the galaxy that is larger than the velocity dispersion is the clearest signature [of tidal destruction]".

4.6. *Implications of Widely Separated RV-Members*

Figures 5 and 8 show that we have found RV-verified Carina member stars to 4.5 r_{lim}. This limit may extend to 4.9 r_{lim} if we adopt a 3σ limit for RV-members specific to the outermost bins in Figure 11, in which case star C2050415 (represented by the outermost square in Figures 5b and 8) is the outermost detected Carina giant. If the RV member at 4.5 r_{lim} is bound to Carina, it sets a new lower limit for the physical extent and tidal radius of the dSph at 96.5 arcmin, or 2.84 kpc for an assumed distance of 101 kpc to Carina (Mateo 1998). Using this radius in the tidal limit equation (Oh et al. 1992):

$$R_{tidal} = a \left(\frac{M_{\rm dSph}}{M_{\rm G}} \right)^{1/3} \left\{ \frac{(1-e)^2}{[(1+e)^2/2e]\ln[(1+e)/(1-e)]+1} \right\}^{1/3} \quad (3)$$

where a is the orbital semimajor axis, $M_{\rm dSph}$ and $M_{\rm G}$ are the mass of the dSph and the MW inside a respectively and e is the orbital eccentricity (values for a and e taken from Piatek et al. 2003 to be 61 kpc and 0.67 respectively), the lower limit to the Carina mass becomes 2.7×10^9 M$_\odot$ assuming a mass of the Milky Way interior to a of $M_{MW} = 6.7 \times 10^{11}$ M$_\odot$ (Burkert 1997). This estimated mass limit is further underestimated because we are taking the *projected* radius of the

star as the actual, three-dimensional distance from the center. Given the Carina luminosity $L = 0.43 \times 10^6$ $L_\odot$ (Mateo 1998), the above mass translates to a global mass-to-light of $M/L > 6,300$, which is more than 100 times higher than the central and total M/L derived for Carina in §4.4 [18]. On the other hand, if the star at 4.9 r_{lim} is a Carina member and it is bound, it sets the tidal radius at 133.7 arcmin, or 3.93 kpc, enclosing an astounding mass of 7.2×10^9 $M_\odot$, which yields $M/L > 16,000$.

While some stars on trapped orbits can be found well outside the true tidal radius up to $2r_{lim}$ or even more (see, e.g., discussion in §7.3 of Binney & Tremaine 1987), the number should be extremely rare beyond $4r_{lim}$. Also, were one to expect the M/L of a galaxy to grow with radius, the asymptotic values implied for Carina are unreasonable high even when compared to values for galaxy clusters: 200 - 300 (Carlberg et al. 1997), which are thought to be approaching fair samples of the universe. From this line of reasoning, we must therefore conclude that either Carina has an enormous, extended dark matter halo to create a M/L an order of magnitude higher than the universe, or, more simply, that these widely separated Carina stars are simply not bound.

We (Muñoz et al. 2005) have used similar arguments in our discussion of the Ursa Minor dSph, where a global M/L of 1,400 to 14,400 was implied by the widest separated RV member, depending on the use of circular or elliptical radii, respectively. While the possibility that the widely separated Muñoz et al. Ursa Minor stars could be interlopers that just happen to have the same RV and color-magnitude positions (i.e. approximate distances) as Ursa Minor was explored and shown to be very unlikely, this miniscule possibility cannot presently be completely discounted. However, the case for the widely separated Carina stars being interlopers is far more difficult to make because of the sheer number of them: six (possibly eight) farther than $2r_{lim}$. Figure 13, which shows the global mass and M/L implied for Carina as progressively more widely separated RV members are attributed as bound satellite members, demonstrates that the implication of an enormous implied Carina M/L is robust to the invalidation of any particular star, or even several, attributed as a sample interloper. The M/L's in Figure 13 are derived in two ways that make use of equation 3: (1) The implied mass of Carina is found by assuming a spherical potential for the dSph and the star's linear projected distance from the center of Carina used as R_{tidal} (*open circles*; again, this is a conservative lower limit, because we are working with *projected* radii). (2) Assuming that the distribution of stars around Carina maintains a constant ellipticity with radius, we can assume there exists for every star not on the major axis a counterpart at the same *elliptical radius* on the major axis which is then used for R_{tidal}. This assumption raises the lower limits on the implied M/L's (*solid circles*). The two methods for deriving the minimum implied M/L probably span the actual limits, since galaxy potentials tend to be rounder than their density profiles.

Figure 13 demonstrates that all of the stars with r_e or R exceeding $0.8r_{lim}$ would need to be discounted as Carina-associated to bring the global minimum M/L to more standard values for the Carina dSph (such as the $M/L \sim 40$ found from core fitting with the central velocity dispersion in §4.4). In other words, if one assumes that the global M/L of Carina is that obtained using the central velocity dispersion, then the tidal boundary *coincides* with the radius at which the break in the density distribution is indeed observed.

Figure 5b attests to the relative purity of the Carina dSph giant candidate sample created by our dual photometric selection criteria (Figs. 3a and 3b): Very few RV outliers are found among our Carina giant candidates overall, and, in addition the small number of giant candidates we find that do *not* share the Carina dSph RV lie predominantly in the 332 km s^{-1} group. Furthermore, Figure 5b suggests that the outer halo is highly substructured (at least when traced by giant stars), a result that is also evident from Figure 2 in Muñoz et al. (2005). In such circumstances, to obtain substantial contamination in our survey would require a considerably unfortunate conspiracy of phenomena to produce a *second* halo substructure with the same RV, approximate distance, and CMD distribution as Carina; we consider this possibility as unlikely.

5. THE CASE FOR TIDAL DISRUPTION OF THE CARINA DSPH

Taken alone, Figure 13 can be argued as a validation of the notion that dSphs like Carina are surrounded by large dark matter halos (Stoehr et al. 2002; Hayashi et al. 2003). According to Hayashi et al. (2003), NFW-like halos that fit the Carina central velocity dispersion (adopted as 6.8 km s^{-1}) and central luminous King profile, even in the face of substantial tidal stripping of the dark halo, still maintain halos with (1) maxima in their circular velocity profile exceeding 50 km s^{-1} that peak well outside r_{lim}, as well as (2) true tidal radii of 11 kpc or more. Making similar arguments for all of the Milky Way satellites alleviates — *at the high mass end* — the mismatch between the CDM-predicted subhalo mass function and that presented by the Galactic satellite system (i.e., the "missing satellites problem"; Kauffmann et al. 1993; Klypin et al. 1999; Moore et al. 1999).

Nevertheless, we believe that an alternative explanation of Figure 13 — i.e. that Carina (and other dSphs) are surrounded by populations of *unbound* stars released through tidal disruption — is not only simpler but also provides a better match to *all* of the available observations of Carina:

Density profile: We have remeasured the Carina density profile with new data, and confirm the existence of a two-component, "King+power law break" shape suggested earlier by the photometric studies of IH95, Kuhn et al. (1996), Paper II, and Monelli et al. (2003, 2004). This photometric work is now solidly backed by spectra of stars in the break population (see also Paper VI), proving the existence of RV-members in the extended power-law break population and leaving no doubt as to the reality of the feature (cf. Morrison et al. 2001; Walcher et al. 2003). This density profile matches (1) the classic shape of a disrupting dSph galaxy, as seen by N-body simulations of disrupting satellites (e.g., Johnston et al. 1999, Mayer et al. 2002) as well as (2) profiles observed in archetype examples of tidal disriuption like the Sagittarius system (Majewski et al. 2003). In contrast, no published dark halo models predict a dynamical structure that would give rise to the observed *luminous*, two-component profile of Carina. It is difficult to imagine how the required structural transition between two bound, pressure-supported stellar populations[19] could be produced so deeply inside an

[18] These estimations are robust to the uncertainties in the orbital parameters derived by Piatek et al. (2003). Their 95% confidence range for e is (0.26; 0.94) which results in a M/L range of (370; 470,000). Even a value for e of 0.24 corresponding to an orbit with peri:apoGalacticon of 63:102 kpc, (their 95% confidence bounds for these parameters) yields a M/L that is an order of magnitude higher than the central value.

[19] We find little evidence for rotation in either the King profile or power law components of the structural profile of Carina within r_{lim}.

extended dark matter halo, and, coincidentally, exhibit *no significant change* in the observed dynamics (velocity dispersion) at this point (see below). Moreover, the position of the break in the profile precisely matches that expected for a Carina having a constant M/L given by the core-fitting technique (§4.4).

Azimuthal configuration: The distribution of stars found in the outer Carina structural component shows a preference to lie along the major axis, and to have an even greater ellipticity than the Carina core, just as would be expected for emerging tidal tails (e.g., Oh et al. 1995; Piatek & Pryor 1995; Johnston et al. 2002; Choi et al. 2002). In contrast, CDM halos tend to have rounder potentials (Stoehr et al. 2002; Hayashi et al. 2003; Bailyn & Steinmetz 2005) so that either the Carina halo is very unusual, or an explanation is required for why its embedded luminous component has a rather different spatial distribution than its dark halo.

Velocity shear: As pointed out in §4.5, the observed velocity trend observed in the Carina system is that expected for tidally induced shear. However, we regard this observed trend with caution appropiate to the still meager statistics for this measurement in the outermost parts of Carina.

Velocity dispersion profile: We find a Carina velocity dispersion profile that is flat and then rising well past the King limiting radius. A characteristic of bound populations is that eventually the velocity dispersion of stars should decline with radius, eventually approaching 0 km s^{-1} at radii where bound stars reach the apocenters of their internal orbits. That a dynamical "cold point" radius is *not reached* even among our most widely separated RV-members suggests that, if bound, these stars are not near the tops of their orbits, and that the tidal radius of Carina must be beyond — even *well beyond*, given the still large velocity dispersion at $\sim 2.5 r_{lim}$ — the observed typical radius of our RV-members. Thus, to explain the observed velocity dispersion trend requires an extremely extended dark halo of even larger dimensions and mass than implied by Figure 13.

In contrast, flat (and rising) dispersion profiles are a natural product of tidal disruption models (Kroupa 1997, M06).

Flattening of the velocity distribution: As shown in recent studies (Mashchenko et al. 2005b; Walker et al. 2005; M06) if the Milky Way tidal field strips stars from dSphs (even if surrounded by a DM halo) the velocity distribution at large radii deviates from a pure Gaussian, in general becoming more platykurtic near and beyond r_{lim}. We have shown for the case of Ursa Minor, Draco (Muñoz et al. 2005), Sculptor (Westfall et al. 2006) and Leo I (Sohn et al. 2006) that the velocity distribution evolves from Gaussian in the center to a flatter distribution with increasing radius. The same is observed in Carina, where the distribution seems to flatten out at large radii, with a kurtosis excess of $\gamma_2 = -0.9 \pm 0.6$ for stars beyond $0.8 r_{lim}$ contrasted with the near-Gaussian $\gamma_2 = +0.2 \pm 0.2$ for stars inside $0.8 r_{lim}$. However, we note that such flattened outer RV distributions could also be observed in systems where the orbits are mostly circular (Dejonghe 1987).

An emerging "too many satellites problem"?: §4.6 makes the case that to keep all of Carina RV members bound requires a potential minimum mass for the dSph of $\sim 1.0 \times 10^9$ M$_\odot$. Muñoz et al. (2005) have performed a similar analysis on the Ursa Minor dSph system and find that to keep it's most widely separated RV-member bound requires a minimum mass of almost 10^9 M$_\odot$, or 10^{10} M$_\odot$ for a counterpart of that star moved along its elliptical isopleth to the major axis. Read et al. (2005b) argue that, in fact, dSphs have masses of 10^9 – 10^{10} M$_\odot$, which would prevent them from undergoing tidal stripping, even in very extreme, radial orbits. Such $\sim$LMC-mass dark matter halos (DMH) are at the limits of the largest subhalo sizes predicted by ΛCDM (Mashchenko et al. 2005a); the existence of *several* $\sim$ *LMC*-mass subhalos in a Milky Way-sized system is not expected (see Figure 14 of Hayashi et al. 2003). If more examples of subhalos much more massive than previously inferred are found — e.g., if we continue to extend the radius over which RV-members are identified in Carina and the other satellites of the Milky Way (see, e.g., §6) and attribute these stars as bound to the dSph — a new problem for CDM will emerge, namely an *excess* of inferred massive satellites about the Milky Way. While the situation is not yet extreme enough to rule out the extended dark halo hypothesis on this basis, nevertheless, it is worth pointing out again that tidal disruption is a simple way to put stars at any arbitrary angular separation from a dSph, should even more extreme outliers be found. Moreover, as Read et al. (2005b) point out, inferring the existence of these extremely extended halos and large masses for satellite galaxies brings an inconsistency with the actual measured central velocity dispersions (which are lower than predicted), even if significant tidal stripping and shocking are considered.

The Sagittarius paradigm: All of the observed spatial and dynamical features in Carina are also found in the one undisputed case of dSph tidal disruption in the Milky Way — the Sagittarius dSph (see Sgr spatial and velocity properties given in Majewski et al. 2003, 2004a). Moreover, we (M06) have explored N-body simulations of modest mass, one component dSph systems (originating as Plummer models) orbiting for significant fractions of a Hubble time and can reproduce the observed properties of Carina fairly well. That *both* (1) an actual, uncontested, *tidally disrupting* analogue of the Carina system, as well as (2) successful tidal disruption models (with fewer unexplained details than alternative, extended dark matter halo models) exist makes it difficult to avoid the question: Is Carina simply another example of the established Sgr paradigm?

Commonality of disruption: A number of discoveries of apparent halo moving groups or streams have recently been made (including the one presented here in the foreground of Carina, see §6): the Monoceros/GASS stream (Newberg et al. 2002; Ibata et al. 2003; Rocha-Pinto et al. 2003; Crane et al. 2003), the TriAnd structure (Rocha-Pinto et al. 2004, Majewski et al. 2004), the M31 giant southern stream (Ibata et al. 2001) and a recently discovered, second M31 halo substrucutre (Kalirai et al. 2005), the identification of an outer Galactic halo stream using blue horizontal branch stars by Clewley et al. (2005), a potential system in Virgo (Duffau et al. 2006); and a new halo moving group found with M giant stars (Majewski et al., in preparation). This growing list of examples provides increasingly solid evidence of a highly substructured Milky Way halo, and to the *commonality* of tidal disruption of stellar systems in the Milky Way halo (e.g., Font et al. 2006; Bullock & Johnston 2005). Such tidal streams must come from *somewhere* and dSph satellites are the most obvious available source.

6. DISCOVERY OF A DYNAMICALLY COLD MOVING GROUP IN THE CARINA FOREGROUND

6.1. *Observed Properties of the 332 km s^{-1} Group*

The new MIKE RVs have revealed an additional coherent RV peak in the field centered on the Carina dSph (Fig. 5) at $v_{hel} = 332.2 \pm 2.6$ km s^{-1}, represented by 15 stars with the

rather small velocity dispersion of 9.8 ± 1.9 km s^{-1} (Figs. 5 and 6). The extreme RV of this system (+122 km s^{-1} when converted to the Galactic Standard of Rest) implies a strong retrograde motion for these stars if they are nominal Milky Way stars at this Galactic position ($[l,b] = [260,-22]^\circ$). The strong RV coherence of this group makes it even more unlikely that it is from a dynamically hot, well-mixed, random Galactic halo population, but the dispersion is, however, of order what one sees in dwarf satellite galaxies: For example, the dispersion is comparable to those measured in the extended parts of the Carina system (Fig. 11) — which we have argued to be likely tidal debris — as well as those measured all along the trailing tidal arm of the Sgr dwarf debris stream (Majewski 2004b). However, the lack of any spatial concentration of these stars across the relatively large span of our survey fields (see Fig. 8b) and their very low apparent density (a factor of ~ 2 more diffuse than the mean $r > r_{lim}$ giant star density for Carina stars of the same apparent magnitude) suggest that these stars represent either tidal debris from a satellite galaxy or an extremely low density part of a very extended satellite.

Figure 14a shows the distribution of stars in this moving group within the CMD of all stars selected to be giants in our photometric survey (according to the tenets of Figure 3b), along with the "Carina dSph RGB" boundary we have used in Figure 3a. The CMD positions of the fifteen 332 km s^{-1} group stars is both highly concentrated and slightly brighter in mean RGB position than the mean CMD locus of the Carina RGB. A similar concentration is also seen for the moving group members in the 2CD (Fig. 14b)[20]; moreover, their relative position in the 2CD compared to Carina stars suggests that the 332 km s^{-1} stars are more metal rich than the mean Carina star (see Paper I), assuming similar [Mg/Fe] ratios.

An independent test of the relative metallicities of these stars comes directly from the spectra: Despite the relatively low S/N of the spectra (which were taken for RVs), in many cases the strong calcium infrared triplet lines are clear. When possible the equivalent width for each triplet line within each MIKE spectrum was measured. We found that for all three calcium lines the equivalent widths for the 332 km s^{-1} group stars were about double those of Carina stars with a similar $(M-T_2)$ color.

We also used a photometric bandpass method for measuring the calcium infrared triplet line strengths because (1) it is perhaps more reliable for relatively low S/N spectra, (2) it averages results over three lines, and (3) a formalism exists to convert these photometric line measures into a formal [Fe/H] value. We limit this work to MIKE spectra with $S/N \geq 7$ per pixel and follow the bandpass definitions summarized in Armandroff & Zinn (1988). We point out that since our original survey was not intended to measure metallicities, we did not observe an appropriate set of stellar calibrators of the metallicity scale. However, since a primary intention is to compare the relative metallicity between the Carina and 332 km s^{-1} group samples, precise calibration is not necessary. Therefore, we followed the prescription outlined in Cole et al. (2004) for converting calcium equivalent width and stellar gravity to [Fe/H], adopting the calibration for this procedure from Koch et al. (2006). A. J. Cenarro graciously made available the code used to measure the line strength indices (Cenarro et al. 2001a,b). For studies of resolved galaxies and star clusters an RGB star's CMD position relative to the system horizontal branch, $V-V_{HB}$, is often used as a proxy for surface gravity. To adopt this method, transformation equations from Majewski et al. (2000a) are used to translate the Washington photometry into Cousins V and I magnitudes. We start by assuming all stars are at the same distance as the Carina dSph and adopt V_{HB}=20.8 as the mean magnitude of the Carina red horizontal branch. Frinchaboy et al. (2005) use a similar technique to study open clusters with spectra having only slightly better S/N and derive a mean metallicity error of 0.3 dex. Therefore, we believe that 0.5 dex is a conservative estimate of our mean uncertainty, where the main contribution comes from uncertainties in the equivalent width measurements.

Figure 15 shows the [Fe/H] distribution derived for both Carina and 332 km s^{-1} group stars under the assumption of a similar distance. The mean [Fe/H] derived for Carina stars is -1.86 with a dispersion of $\pm$0.41 — in good agreement with other studies (Monelli et al. 2003; Koch et al. 2006) — whereas the mean [Fe/H] derived for the 332 km s^{-1} group is -0.93 with a dispersion of $\pm$0.62. Barring possible variations in [Ca/Fe] between the two groups of stars, Figure 15 suggests that the metallicity of the moving group may be ~ 0.9 dex higher in [Fe/H] than the Carina dSph were this group at the same distance.

6.2. *The Magellanic Cloud Connection*

On the other hand, if these moving group stars are more metal rich (as their calcium line strengths suggest), they are also *intrinsically fainter* in the V band, whereas they are also *brighter* in apparent magnitude relative to Carina stars of the same color. All of this suggests that the moving group must be *closer* than Carina, and by as much as a magnitude in distance modulus or more (see, e.g., Fig. 12a of Paper I). Interestingly, this places the distance of these stars to be of order the distance of the Large Magellanic Cloud (LMC), *the center of which not only lies only* $\sim 20^\circ$ *away from the center of our Carina field in the sky but has a similarly high systemic heliocentric velocity (262 km s*$^{-1}$*; van der Marel et al. (2002, hereafter vdM02)*. Even more intriguing, in other $M,T_2,DDO51$ photometric survey work in fields encircling the LMC we have found additional giant stars with LMC-like velocities ranging from 4 to 18.5° away from the LMC center in the general region between the LMC and the Carina dSph. Preliminary results for this work have been shown in e.g., Fig. 6 of Majewski (2004), and a more complete discussion will be given elsewhere (Nidever et al., in preparation). Here we focus on the relative positions (Fig. 16) and velocities (Fig. 17) of our best-quality velocities for stars in fields that bridge the region between the LMC core and our Carina survey field. Because the expanse of sky involved is sufficiently large that there is significant variation in the reflex motion of the Sun in the RV, Figure 17 shows velocities after conversion to the Galactic Standard of Rest (GSR) frame.[21] [22]

After conversion to v_{GSR}, an even greater agreement is found (Fig. 17) between the actual velocities of the LMC (big solid circle), the 332 km s^{-1} group in the Carina field

[20] Note that two of the fifteen moving group stars lie just outside our more conservative giant selection criteria, and were part of the experimental foray into this region with the MIKE sample discussed in §3.1.

[21] Figure 17 shows *all* giant candidates in our survey regions with measured RVs within the plotted v_{GSR} range; groups of stars with clumped, negative (i.e. generally retrograde) v_{GSR} are also found (e.g., see Majewski 2004b), but are not relevant to the present discussion.

[22] The adopted motion of the Sun is (232,9,7) km s^{-1} in the Galactic rotation, anticenter and Z directions.

(smaller filled circles), and RGB stars we have found with similar velocities between these systems (open triangles and circles). While the relative numbers of stars in each position on Figure 17 are a function of widely varying survey areas, spectroscopic magnitude limits, and spectroscopic target selection (i.e. whether or not stars were selected to be an LMC-like giant, a Carina-like giant, or any kind of giant); what is relevant is the smooth variation of the mean velocities in each survey field from the LMC to the 332 km s^{-1} group, a trend that strongly suggests a dynamical association of all of these stars.[23] Even more intriguing is that this velocity trend matches that found for other LMC tracers (e.g., Schommer et al. 1992; Kunkel et al. 1997b) at similar position angles from the LMC core over a 13° angular separation from the LMC center, and where the trend is attributed to the rotation curve of the LMC (Schommer et al. 1992; Kunkel et al. 1997b; vdM02).

Figure 17 shows the RV trend for the LMC disk (solid line) and halo (dashed line) from the best-fitted model to previously published outer LMC data by vdM02 (see their Fig. 5). We show the trends at LMC position angles corresponding to our survey fields and to the 13° limit of the model and previous data, as well as an extrapolation of the vdM02 LMC RV trends to the Carina field.[24] This figure suggests that the inner data follow the disk velocity trend, whereas the 332 km s^{-1} moving group lies right on the extrapolation of the halo velocity trend to $\sim 22°$ (~ 20 kpc) radius from the LMC center.

To further test an association of the Magellanic Clouds to the 332 km s^{-1} group stars, we compare in Figure 18 their distribution in the CMD and 2CD to that of stars found in the closest survey field to the LMC, shown by a green open circle in Figure 16. The position of spectroscopically-confirmed LMC stars from this same inner RV survey field are shown by green open triangles in Figure 18. Figure 18a shows that the CMD position of the 332 km s^{-1} group stars (red solid circles) is *precisely* where the locus of the LMC's prominent red clump slightly overlaps our Carina RGB selection boundary. Moreover, inspection of our Carina field sample of giant stars that fall outside our Carina CMD selection region in Figure 14a reveals: (1) a possible additional concentration of stars at $M_0 \sim 19$ just outside the Carina selection boundary at the position of the LMC red clump seen in Figure 18a (although not stretching as blueward in Fig. 14a because such stars are eliminated by the 2CD selection); and (2) a slight excess of stars tracking the nominal position of the LMC RGB visible in Figure 18a, above the Carina RGB selection boundary. To test whether both of these groups of "Carina outliers" may be Magellanic in origin, on UT 2005 August 15 we observed two bright giant candidates in this "LMC RGB position" of the CMD (marked as solid squares in Figure 18) using the MIKE spectrograph on the Magellan telescope. These turned out to have RVs (317 and 342 km s^{-1}) consistent with membership in the 332 km s^{-1} group, which further vindicates a Magellanic Cloud provenance of this moving group.[25] Comparison of Figures 14a and 18a certainly evokes the notion of a diaphanous presence of LMC stars in the foreground of the Carina dSph, which has given rise to the 332 km s^{-1} group. Finally, within the GIRAFFE RV dataset, we found four more stars with velocities matching the 332 km s^{-1} group and positions in the CMD (red open circles in Figure 18) reasonably compatible with being LMC red clump stars. Adding these four stars changes only marginally the mean velocity and the velocity dispersion of the moving group.

With the possible connection to the Magellanic Clouds in mind, we can bring the abundance argument full circle to look for self-consistency of this hypothesis. For example, if the originally identified 332 km s^{-1} group members are parts of the red clump of the LMC, then for each star we can recalculate its [Fe/H] from the infrared triplet strength assuming the V_{HB} = 19.2 of the LMC red clump. The result yields a mean [Fe/H]=-0.67 (with dispersion ± 0.62 dex) — relatively more metal poor than, but still consistent with the mean metallicity ([Fe/H]=–0.37) of the dominant population of stars in the LMC found recently by Cole et al. (2005) using the same infrared triplet methodology. Considering also that it would seem unlikely to find two such extreme velocity stellar systems at a similar distance and position in the sky, the collective evidence compellingly suggests that we have found widely dispersed stars from one of the Magellanic Clouds — the LMC being more likely — in the foreground of the Carina dSph.

6.3. *Implications for LMC Structure*

As with the examples of the Carina dSph explored earlier, and the Ursa Minor system explored in Muñoz et al. (2005), the presence of extremely widely displaced, but satellite-associated stars would seem to have profound implications for the structure of the LMC. One can use equation (45) from vdM02 to estimate the mass of the LMC given a certain tidal radius. For our most widely separated star in the 332 km s^{-1} group ($\sim 22°$ away from the center of the LMC) to remain bound to the LMC implies a minimum LMC mass of 3.1×10^{10} $M_\odot$ assuming a Milky Way mass interior to the LMC of 4.9×10^{11} $M_\odot$ (Kochanek 1996; the Burkert 1997 model gives almost the identical Milky Way mass). This inferred LMC mass is ~ 3.5 times more than that reported by vdM02 (8.7×10^9 $M_\odot$) to a 13° radius and consistent with the 2.0×10^{10} $M_\odot$ LMC mass derived if we assume a flat LMC rotation curve to this distance. The implied 20.2 kpc minimum tidal radius is now more than 33% (1σ) greater than the 15.0 ± 4.5 kpc tidal radius estimated by vdM02.

These results immediately suggest two possible scenarios (ignoring possible solutions offered by Modified Newtonian Dynamics; Milgrom 1995; Sanders & McGaugh 2002): (1) The LMC is substantially larger than previously appreciated. The inferred total M/L would exceed 10 in solar units. An even larger mass is implied by the fact that the velocity dispersion of the 332 km s^{-1} — 9.8 km s^{-1} — while $\sim 2\times$ smaller than the dispersions of tracers < 10 kpc from the LMC, as might be expected in the outer limits of a galaxy halo, are still quite larger than the expected, small asymptotic value at the "edge" of a galaxy.[26] We note that an LMC extending out to ~ 20 kpc (in the line of sight) has been already proposed by Zaritsky & Lin (1997) based on the identification of

[23] An apparent difference in the velocity dispersions among the different sets of points in Figure 17 is in part attributable to the more than $5\times$ lower RV precision of the measurements for the stars found outside the Carina survey region.

[24] The model in Figure 17 should not be interpreted as the actual rotation curve, but a velocity trend on the sky. The actual rotation curve corresponding to these points is shown in Figure 6 of van der Marel et al. (2002).

[25] We note the RV uncertainties for these stars are large, ~ 15 km s^{-1}, therefore we do not include them in the velocity dispersion calculation but only use them as membership information.

[26] While RVs for stars in our analysis that lie outside the Carina field are generally of lower resolution, the velocity dispersions for our fields less than 10° match well those found for the carbon stars summarized in Figure 6 of vdM02.

a vertically extended red clump in the CMD of a field in the direction of the LMC. (2) The Magellanic Cloud stars we observe in the foreground are not bound to the LMC. The colder dynamics of the 332 km s^{-1} stars might be explained through a tidal debris origin.

But if unbound, stars in the direction of the Carina dSph are *not* aligned with the expected direction of an LMC tidal tail, based on both the typical proper motions[27] measured for the LMC (summarized in Table 1 of vdM02) as well as the direction of the HI Magellanic Stream (both the leading and trailing arms) — both lie in a roughly orthogonal direction. This is not necessarily a problem, since stars will be tidally stripped anywhere along the satellite-Milky Way equipotential, whereas we have only explored one position angle from the LMC here. On the other hand, the Carina survey field *does* happen to lie more or less along the axis defined by the LMC and SMC. A tidal disruption scenario involving an interaction of the LMC and SMC might conceiveably throw Magellanic stars out along this axis. For example, the velocities of our Magellanic giant stars are consistent with those of the carbon stars found by Kunkel et al. (1997a,b) in the same general direction (see Figs. 16 and 17), and which these authors attribute to a "polar ring" of SMC debris around the LMC. Alternatively, the widely separated "LMC" stars may constitute residue from the disruption of a former "Greater Magellanic Galaxy" which has often been invoked as a possible explanation for the curious alignment of a number of Milky Way satellites and globular clusters along a "Magellanic Plane" that also includes the HI Magellanic Stream (Kunkel 1979, Lynden-Bell 1982, Majewski 1994, Fusi Pecci et al. 1995, Lynden-Bell & Lynden-Bell 1995, Majewski et al. 1996, Palma et al. 2002). A dynamical association of Ursa Minor, Draco, the LMC and the SMC is suggested by their common motions along one great circle (see, e.g., Fig. 3 of Palma et al. 2002). Were this group of Milky Way satellites truly daughters of the break up of a Greater Magellanic system or produced together as tidal dwarfs during a major merger with the Milky Way, their close, but not precise, alignment in a single plane might indicate the possibility of a potentially broad stellar swath of loosely coherent Magellanic Plane debris. But if the 332 km s^{-1} stars represent dynamically *old* tidal debris like this, one might not expect it to so well match the current distance of the LMC, nor its velocity (or, even more coincidentally, the velocity extrapolated from the LMC velocity trend to this position in the sky).

Only with further surveying for additional "332 km s^{-1} group" stars in other directions around the Magellanic Clouds can one hope to test such hypotheses. We intend to explore these possibilities further elsewhere (Nidever et al., in preparation) with a larger database of outer LMC stars collected over a larger area.

7. SUMMARY AND DISCUSSION

Our survey for diffuse halo substructure in a large field around the Carina dSph has yielded the following primary results on the structure of both the Carina dSph and the LMC (or Magellanic Clouds):

— Using a combination of new Washington+*DDO*51 photometry and new echelle spectroscopy we have confirmed the existence of an extended, power law component in the density distribution of Carina, which can be modeled as a "King + power law". Such density distributions are characteristic of those found in models of disrupted satellites and has also been observed in the tidally disrupting Sgr dSph.

— With Magellan+MIKE echelle spectroscopy of giant star candidates in the Carina field we have establish the existence of Carina stars to the limits of our photometric survey field, with confirmed Carina members to at least $4.5r_{lim}$, and likely $4.9r_{lim}$. These detections represent the most widely separated stars (in terms of r_{lim}) found associated with any dSph (apart from the Sgr dSph) to date. Beyond verifying the existence of the extended Carina population, these widely separated member stars have profound implications for the structure of Carina: If the stars are bound, Carina must have a minimum total M/L of 6,300 in solar units, or 16,000 in the case of the $4.9r_{lim}$ example.

— With the addition of VLT+GIRAFFE spectroscopic data and other published data (Mateo et al. 1993; Paper VI) within r_{lim} to our MIKE velocities at large r_{lim}, we have good and continuous sampling of the Carina RV distribution to well past r_{lim} by 408 confirmed Carina members. With these data, we have rederived the central and global M/L for Carina, assuming a single-component model and using the core-fitting technique; the results yield 43^{+53}_{-19} and 41^{+40}_{-25} $(M/L)_\odot$ respectively, where the main source of uncertainty comes from the luminosity. These results are significantly at odds with the lower limits to the global M/L found using the outlying Carina members above.

— With the extensive RV coverage we have also derived the line of sight radial velocity dispersion profile for Carina to $\sim 2.5r_{lim}$, the most extensive such profile so far (by more than a factor of two) for any dSph. The profile is flat to past r_{lim} and then exhibits a rise in the dispersion to almost twice the inner value at $> 2r_{lim}$. Such results are incompatible with completely bound, mass-follows-light dSph models, but also challenge two-component models that account for the flat dispersion via an extended dark halo surrounding the dSph. In the latter case an enormous halo is needed, one significantly more massive than that implied above for simply keeping the $> 4r_{lim}$ Carina stars bound, since the significant dispersion at large radius implies that the tidal radius is much farther out.

— While with our new data we cannot definitively rule out a *very* large, and extended dark halo for Carina — one producing a global M/L approaching as much as 6,300 or more — we conclude that a simpler, less contrived scenario that provides a good match to *all* available observations of Carina is that it is tidally disrupting and we have identified some of its unbound stars. This scenario simultaneously accounts for the following observed features of the Carina system: (1) Its "King+power law" density profile, which is a natural product of tidal disruption; (2) the fact that the extended component of Carina lies predominantly along its major axis and shows increasing ellipticity with radius, as would be expected in nascent tidal tails; (3) Carina stars extending from the core to the edge of the survey area; (4) the flat, then rising velocity dispersion profile with radius; and (5) a flattening of the RV distribution with radius, from Gaussian in the core to platykurtic at large radius. Explaining this combination of observed Carina properties with extended dark halo scenarios will require substantial efforts to create successful ad hoc models. On the other hand, all of the above Carina features not only resemble those seen in the established, tidally

[27] We must note that this may not be a problem if the LMC had a significantly different proper motion. In particular, Momany & Zaggia 2005 argue that the LMC is in fact moving in the direction of Carina, but warn the reader that there are likely to be unidentified systematic errors in the UCAC2 that they used that are responsible for these results.

disrupting Sgr dSph system, but have been well-matched by mass-follows-light models (presented in a companion paper, Muñoz et al. 2006) of disrupting dSphs having the nominal central $M/L \sim 40$ derived here.

— Finally, we have detected a second, strongly velocity-coherent structure in the Carina field with even higher RV than Carina. The more metal rich stars constituting this moving group have CMD positions consistent with LMC red clump stars and their velocities follow the extrapolated velocity trend expected for LMC halo stars. With additional Washington+*DDO*51 photometry and follow-up spectroscopy we have traced this population from 4° separation from the center of the LMC out to the 22° separation of the Carina field center. These stars either represent the detection of Magellanic stellar tidal debris, or, if bound to the LMC, imply a significantly larger mass and tidal radius for the LMC than previously determined.

Traditionally, debate over the kinematical and structural properties of the diffuse, low surface brightness dSphs has tended to polarize around two primary interpretations: (1) that dSphs are dark matter dominated (e.g., Mateo 1998) galaxies, with M/L reaching to as much as 100 $(M/L)_\odot$, making them structurally different compared to globular clusters and dE systems. The prime observational evidence to support this claim is the relatively high measured central velocity dispersions that — coupled with an assumption of dynamical equilibrium — imply masses far in excess of that inferred by the luminous component. Alternatively, (2) dSphs have also been discussed as systems partly or completely out of virial equilibrium (Hodge & Michie 1969; Kuhn & Miller 1989; Kuhn 1993; Kroupa 1997; Gómez-Flechoso et al. 1999; Fleck & Kuhn 2003). Such an assertion seeks to explain the large central velocity dispersions of dSphs through inflation by tidal heating or other dynamical effects, allowing for much more modest dSph masses, consistent with no dark matter.

To date, despite much observational and theoretical effort, the physical evidence has generally remained unpersuasive enough to dislodge the most ardent adherents to these models. Reinforcing viewpoints have been several "all or nothing" notions introduced into the debate, including: (1) the assumption that dark matter dominated systems are in dynamical equilibrium throughout their entire physical extent (e.g., Stoehr et al. 2002; Walker et al. 2005); or, (2) if evidence of tidal stripping is found around a dSph, the system must be devoid of dark matter (e.g., Burkert 1997).

Remarkably, more recent work intended to *clarify* the physical nature of dSphs has, instead, increased the apparent gulf between diametrical viewpoints. Kleyna et al. (1999) had previously suggested that "only $\sim 10-20$ additional observations [of dSph star RVs] at 0.75 times the tidal radius would be required to distinguish clearly between an MFL distribution and an extended halo or disrupted remnant model with a flat or radially rising velocity dispersion." Yet, despite the fact that the latest dSphs spectroscopic surveys have provided RVs of hundreds of dwarf members to beyond $0.75r_{lim}$ in several systems (Mateo 1997; Kleyna et al. 2002, 2004; Wilkinson et al. 2004; Tolstoy et al. 2004; Westfall et al. 2006; Muñoz et al. 2005; Walker et al. 2005; Sohn et al. 2006), we are apparently no closer to a consensus view of dSph dynamics. While this is partly due to technical differences in interpretation of even the same databases (e.g., Wilkinson et al. 2004, Łokas et al. 2005, Muñoz et al. 2005), in general most studies are finding flat dSph velocity dispersion profiles to be the norm. As discussed several times here, such profiles are produced naturally in dSph models undergoing tidal disruption (see also Kuhn & Miller 1989; Kroupa 1997; Mayer et al. 2002, Fleck & Kuhn 2003; Read et al. 2005a; M06). However, rather than settling the issue, these rather flat velocity dispersion profiles have prompted the development of even more extreme, two-component, extended dark halo dSph models with *substantially higher* bound masses and total M/L — exceeding 400 or even 1000 $(M/L)_\odot$ (e.g., Łokas 2002; Kleyna et al. 2002; Walker et al. 2005). These models are partly motivated by the proposition that the so-called missing satellite problem of ΛCDM cosmologies could be alleviated if galactic dSph satellites inhabit the most massive sub-halos — i.e., $M_{dSph} > 10^9$ $M_\odot$, or equivalently $V_{circ} > 30 - 40$ km s^{-1} (Stoehr et al. 2002; Hayashi et al. 2003).[28]

From the numerous arguments laid out thus far, we are persuaded that the weight of evidence militates against the extreme halo hypothesis for Carina in favor of a tidal disruption scenario. Yet one more argument favors the latter hypothesis: An extended DM halo of the magnitude our data would require in this scenario has ancillary implications for the *chemical evolution* of Carina that are problematical. Despite having a complex and episodic star formation history, Carina has a relatively low mean metallicity of [Fe/H]~ -1.9 (Monelli et al. 2003; Koch et al. 2006). Tolstoy et al. (2003) note that galaxy masses of order a few times 10^7 $M_\odot$ — consistent with the mass of Carina derived from central velocity dispesion (Mateo et al. 1993; §4.4) — are low enough to suffer metal-enriched winds, which promote preferential depletion of metals but retention of sufficient gas to allow further star formation at a continued, relatively low mean metallicity (like Carina's). A larger galactic potential diminishes the possibility of blow-out/blow-away of either gas or metals (e.g., Vader 1986, 1987; Mac Low & Ferrara 1999; Ferrara & Tolstoy 2000), leading to closed-box enrichment (Tolstoy et al. 2003). But Koch et al. (2006) find that the metallicity distribution function of Carina is not well matched by a closed-box model. If Carina has an enormous extended DM halo, it would have resulted in an enrichment that it is not observed (Smecker-Hane et al. 1996). However, a more modest Carina dark matter content is not discounted by this argument.

One of our goals in this paper (see also Muñoz et al. 2005) has been to push the measurement of physical parameters in one dSph to hitherto unexplored regions to see if, in at least one system, new data in the extrema can definitively rein in the range of possible models. We conclude that the new breed of extremely large M/L, extended dark matter halos is less likely to apply to the present Carina dSph than a tidal disruption scenario, which more readily explains all present observational data on the satellite.[29] That said, our results do not rule out *any* dark matter in the dSph, and, indeed, as we shall show in Muñoz et al. (2006), an easily workable (and therefore likely) model for Carina is one with elements of

[28] We note, however, that Kazantzidis et al. (2004) argue against this picture, showing that, in the case of Draco and Fornax, only halos of $V_{circ} <$ 25 km s^{-1} can succesfully reproduce the velocity dispersion profiles of these dSphs.

[29] This conclusion does not preclude the possibility that a formerly extended dark halo might have been stripped from Carina at earlier times. Thus, the success of tidally disrupting, mass-follows-light models in describing at least some dSphs (M06, Sohn et al. 2006) could be consistent with ΛCDM if the models produce subhalos that are sufficiently stripped to reach the luminous matter.

both of the originally debated dSph scenarios: a tidally disrupting, mass-follows-light dSph, but one with relatively high ($M/L \sim 35-40$) dark matter content, as suggested by the central velocity dispersion.

It has recently been claimed (Gilmore 2004) that "Sgr was a rare event, not a paradigm for the average". This conclusion has been motivated by the notion that were systems like the Carina dSph tidally disrupting, then the halo should have large numbers of youngish (e.g., blue main sequence) stars in larger numbers than seen (Unavane et al. 1996). Such an analysis presumes that the *present* Carina system is representative of the typical stellar population that would have been contributed to the halo by tidally disrupting dSph systems *including the former Carina*. In contrast, as was previously demonstrated in Majewski et al. (2002), if for a Hubble time Carina were disrupting at the fractional mass loss rate implied by its density profile, — i.e. < 0.24 Gyr^{-1} (see §2.2) — then far more stars from Carina's oldest population would have been lost by now than from either the intermediate-aged or young populations in Carina. This is also a reasonable explanation for why the Carina system today is dominated by it's intermediate-aged population, and even for why there seems to be a radial metallicity and age gradient in Carina: The present balance of populations bound to Carina likely reflects the competing interplay of star formation history and mass loss history (Font et al. 2006) in this disrupting analogue of the Sgr dSph galaxy.

We appreciate useful discussions with David Law and Andrew McWilliam. We thank an anonymous referee for helpful suggestions that helped improve the paper and to Carlton Pryor for providing us with his code to calculate velocity dispersions using the Maximim Likelihood Method. We acknowledge funding by NSF grant AST-0307851, NASA/JPL contract 1228235, the David and Lucile Packard Foundation, and the generous support of Frank Levinson and through the Celerity Foundation. Additionally, P. M. F. is supported by the NASA Graduate Student Researchers Program, a University of Virginia Faculty Senate Dissertation-Year Fellowship, and by the Virginia Space Grant Consortium. D.L.N. is supported by the ARCS Foundation, a University of Virginia President's Fellowship, and by the Virginia Space Grant Consortium.

REFERENCES

Armandroff, T. E., & Zinn, R. 1988, AJ, 96, 92
Armandroff, T. E., Olszewski, E. W. & Pryor, C. 1995, AJ, 110, 2131
Bailyn, J. & Steinmetz, M. 2005, ApJ, 627, 647
Binney, J., & Tremaine, S. 1987, in Galactic Dynamics, Princeton, New Jersey
Bullock, J. & Johnston, K. V. 2005, ApJ, 635, 931
Burkert, A. 1997, ApJ, 474, L99
Carlberg, R. G., Yee, H. K. C., & Ellingson, E. 1997, ApJ, 478, 462
Cenarro, A. J., Cardiel, N., Gorgas, J., Peletier, R. F., Vazdekis, A. & Prada, F. 2001, MNRAS, 326, 959
Cenarro, A. J., Gorgas, J., Cardiel, N., Pedraz, S., Peletier, R. F. & Vazdekis, A. 2001, MNRAS, 326, 981
Clewley, L., Warren, S. J., Hewett, P. C., Norris, J. E., Wilkinson, M. I. & Evans, N. W. 2005, MNRAS, 362, 349
Cole, A. A., Smecker-Hane, T. A., Tolstoy, E., Bosler, T. L. & Gallagher, J. S. 2004, MNRAS, 347, 367
Cole, A. A., Tolstoy, E., Gallagher, J. S., & Smecker-Hane, T. A. 2005, AJ, 129, 1465
Choi. P. I., Guhathakurta, P. & Johnston, K. V. 2002, AJ, 124, 310
Crane, J. D., Majewski, S. R., Rocha-Pinto, H. J., Frinchaboy, P. M., Skrutskie, M. F., & Law, D. R. 2003, ApJ, 594, L119
Cuddeford, P. & Miller, J. C. 1990, MNRAS, 244, 64
Dejonghe, H. 1987, MNRAS, 224, 13
Duffau, S., Zinn, R., Vivas, A. K., Carraro, G., Méndez, R. A., Winnick, R. & Gallart, C. 2006, ApJ, 636, L97
Faber, S. M. & Lin, D. N. C. ApJ, 266L, 17
Ferrara, A., & Tolstoy, E. 2000, MNRAS, 313, 291
Fleck, J. & Kuhn, J. R. 2003, ApJ, 592, 147
Frinchaboy, P. M., Muñoz, R. R., Majewski, S. R., Friel, E. D., Phelps, R. L., & Kunkel, W. E. 2005, in "Chemical Abundances and Mixing in Stars in the Milky Way and its Satellites", eds. L. Pasquini & S. Randich, ESO Astrophysics Symposia, *in press* (astro-ph/0411127)
Frinchaboy, P. M., Muñoz, R. R., Phelps, R. L., Majewski, S. R., & Kunkel, W. E. 2006, AJ, 131, 922
Font, A., Johnston, K. V., Bullock, J. & Robertson, B. 2006, ApJ, 638, 585
Fusi Pecci, F., Bellazzini, M., Cacciari, C., & Ferraro, F. R. 1995, AJ, 110, 1664
Geisler, D. 1996, AJ, 111, 480G
Gilmore, G. 2004, in "Milky Way Surveys: The Structure and Evolution of our Galaxy", ASP Conference Proceedings Vol. 317, eds. D. Clemens, R. Shah, & T. Brainerd (San Francisco: ASP), 239
Gómez-Flechoso, M. A., Fux, R., & Martinet, L. 1999, A&A, 347, 77
Hargreaves, J. C., Gilmore, G., Irwin, M. J., & Carter, D. 1994, MNRAS, 269, 957
Hayashi, E., Navarro, J. F., Taylor, J. E.,Stadel, J., & Quinn, T. 2003, ApJ, 584, 541
Hodge, P. W. & R. W. Michie 1969, AJ, 74, 587
Ibata, R. A., Irwin, M. J., Lewis, G. F., Ferguson, A. M. N., & Tanvir, N. 2001, Nature, 412, 49
Ibata, R. A., Irwin, M. J., Lewis, G. F., Ferguson, A. M. N., & Tanvir, N. 2003, MNRAS, 340, L21
Illingworth, G. 1976, ApJ, 204, 73
Irwin, M. & Hatzidimitriou, D. 1995, MNRAS, 277, 1354 (IH95)
Johnston, K. V., Sigurdsson, S. & Hernquist, L. 1999, MNRAS, 302, 771
Johnston, K. V., Choi, P. I. & Guhathakurta, P. 2002, AJ, 124, 127
Kalirai, J. S., Guhathakurta, P., Gilbert, K. M., Reitzel, D. B., Majewski, S. R., Rich, R. M., & Cooper, M. C. 2005, (astro-ph/0512161)
Kauffmann, G., White, S. D. M., & Guiderdoni, B. 1993, MNRAS, 261, 201
Kazantzidis, S., Mayer, L., Mastropietro, C., Diemand, J., Stadel, J., & Moore, B. 2004, ApJ, 608, 663
King, I. R. 1966, AJ, 71, 64
King, I. R. 1962, AJ, 136, 784
Kleyna, J. T., Geller, M. J., Kenyon, S. J. & Kurtz, M. J. 1999, AJ, 117, 1275
Kleyna, J. T., Wilkinson, M. I., Evans, N. W., Gilmore, G. & Frayn, C. 2002, MNRAS, 330, 792
Kleyna, J. T., Wilkinson, M. I., Evans, N. W., & Gilmore, G. 2004, MNRAS, 354, L66
Klypin, A., Kravtsov, A. V., Valenzuela, O., & Prada, F. 1999, ApJ, 522, 82
Kochanek, C. S. 1996, ApJ, 457, 228
Kroupa, P. 1997, New Astronomy, 2, 139
Koch, A., Grebel, E. K., Wyse, R. F. G., Kleyna, J. T., Wilkinson, M. I., Harbeck, D., Glimore, G. F. & Evans, N. W. 2006, 131, 895
Kuhn, J. R. & Miller, R. H. 1989, ApJ, 341, 41
Kuhn, J. R. 1993, ApJ, 409, L13
Kuhn, J. R., Smith, H. A. & Hawley, S. L. 1996, ApJ, 469, L93
Kunkel, W. E. 1979, ApJ, 228, 718
Kunkel, W. E., Irwin, M. J. & Demers, S. 1997a, A&AS, 122, 463
Kunkel, W. E., Demers, S., Irwin, M. J. & Albert, L. 1997b, ApJ, 488, L129
Łokas, E. L., 2002, MNRAS, 333, 697
Łokas, E. L., Mamon, G. A. & Prada, F. 2005, MNRAS, 363, 918
Lynden-Bell, D. 1982, The Observatory, 102, 202
Lynden-Bell, D., & Lynden-Bell, R. M. 1995, MNRAS, 275, 429
Mac Low, M., & Ferrara, A. 1999, ApJ, 513, 142
Majewski, S. R. 1994, ApJ, 431, L17
Majewski, S. R., Phelps, R. & Rich, R. M. 1996, in The History of the Milky Way and Its Satellite System, ed. A. Burkert, D. Hartmann, & S. Majewski, (San Francisco: ASP), 1
Majewski, S. R., Ostheimer, J. C., Kunkel, W. E. & Patterson, R. J. 2000a, AJ, 120, 2550 (Paper I)
Majewski, S. R., Ostheimer, J. C., Patterson, R. J., Kunkel, W. E., Johnston, K. V. & Geisler, D. 2000b, AJ, 119, 760 (Paper II)
Majewski, S. R., et al. 2002, in "Modes of Star Formation and the Origin of Field Populations", ASP Conference Proceedings Vol. 285, eds. E. K. Grebel & W. Brandner (San Francisco: ASP), 199
Majewski, S. R., Skrutskie, M. F., Weinberg, M. D. & Ostheimer, J. C. 2003, ApJ, 599, 1082
Majewski, S. R., et al. 2004a, AJ, 128, 245
Majewski, S. R. 2004b, Publications of the Astronomical Society of Australia, 21, 197

Majewski, S. R., et al. 2005, AJ, 130, 2677
Mashchenko, S., Couchman, H. M. P. & Sills, A. 2005a, ApJ, 624, 726
Mashchenko, S., Sills, A., & Couchman, H. M. P. 2005b, (astro-ph/0511567)
Mateo, M., Olszewski, E. W., Pryor, C., Welch, D. & Fischer, P. 1993, AJ, 105, 510M
Mateo, M. 1997, ASP Conf. Ser. 116: The Nature of Elliptical Galaxies; 2nd Stromlo Symposium, 259
Mateo, M. L. 1998, ARA&A, 36, 435
Mayer, L., Moore, B., Quinn, T., Governato, F. & Stadel, J. 2002, MNRAS, 336, 119
Milgrom, M. 1995, ApJ, 455, 439
Momany, Y., & Zaggia, S. 2005, A&A, 437, 339
Monelli, M., et al. 2003, AJ, 126, 218
Monelli, M., et al. 2004, Memorie della Societa Astronomica Italiana Supplement, 5, 65
Moore, B., Ghigna, S., Governato, F., Lake, G., Quinn, T., Stadel, J., & Tozzi, P. 1999, ApJ, 524, L19
Muñoz, R. R. et al. 2005 ApJ, 631, L137
Morrison, H. L., Olszewski, E. W., Mateo, M., Norris, J. E., Harding, P., Dohm-Palmer, R. C. & Freeman, K. C. 2001, AJ, 121, 283
Newberg, H. J. et al. 2002, ApJ, 569, 245
Odenkirchen, M. et al. 2001, AJ, 122, 2538
Oh, K. S., Lin, D. N. C., & Aarseth, S. J. 1992, ApJ, 386, 506
Oh, K. S., Lin, D. N. C., & Aarseth, S. J. 1995, ApJ, 442, 142
Olszewski, E. W., Pryor, C. & Armandroff, T. E. 1996, AJ, 111, 750
Olszewski, E. W. & Aaronson, M. 1985, AJ, 90, 2221
Osterbrock, D. E., Fulbright, J. P., Martel, A. R., Keane, M. J., Trager, S. C., & Basri, G. 1996, PASP, 108, 277
Osterbrock, D. E., Fulbright, J. P., & Bida, T. A. 1997, PASP, 109, 614
Palma, C., Majewski, S. R. & Johnston, K. V. 2002, ApJ, 564, 736
Piatek, S., & Pryor, C. 1995, AJ, 109, 1071
Piatek, S., Pryor, C., Olszewski, E. W., Harris, H. C., Mateo, M., Minniti, D., & Tinney, C. G. 2003, AJ, 126, 2346
Pryor, C., & Meylan, G. 1993, in ASP Conf. Ser. 50, Structure and Dynamics of Globular Clusters, ed. S. Djorgovski & G. Meylan (San Francisco: ASP), 357
Pryor, C. 1996, ASP Conf. Ser. 92: Formation of the Galactic Halo...Inside and Out, 92, 424
Read, J. I., Wilkinson, M. I., Evans, N. W., Gilmore, G. & Kleyna, J. T. 2005a, (astro-ph/0506687)
Read, J. I., Wilkinson, M. I., Evans, N. W., Gilmore, G. & Kleyna, J. T. 2005b, (astro-ph/0505226)
Rocha-Pinto, H. J., Majewski, S. R., Skrutskie, M. F., & Crane, J. D. 2003, ApJ, 594, L115
Rocha-Pinto, H. J., Majewski, S. R., Skrutskie, M. F., Crane, J. D., & Patterson, R. J. 2004, ApJ, 615, 732
Richstone, D. O. & Tremaine, S. 1986, AJ, 92, 72
Salaris, M. & Girardi, L. 2002, MNRAS, 337, 332
Sanders, R. H. & McGaugh, S. S. 2002, ARA&A, 40, 263
Schommer, R. A., Suntzeff, N. B., Olszewski, E. W., & Harris, H.C. 1992, AJ, 103, 447
Schlegel, D. J., Finkbeiner, D. P., & Davis, M. 1998, ApJ, 500, 525
Smecker-Hane, T. A., Stetson, P. B., Hesser, J. E., & Vandenberg, D. A. 1996, in "From Stars to Galaxies: the Impact of Stellar Physics on Galaxy Evolution", ASP Conference Proceedins Vol 98, eds. C. Leitherer, U. Fritze-von Alvensleben, & J. Huchra (San Francisco: ASP), 328
Sohn, S., Majewski, S. R., Muñoz, R. R., Kunkel, W. E., Johnston, K. V., Ostheimer, J. C., Guhathakurta, P., Patterson, R. J., Siegel, M.H., & Cooper, M. 2006, ApJ, *submitted*
Stetson, P. B. 1987, PASP, 99, 191
Stoehr, F., White, S. D. M., Tormen, G., & Springel, V., 2002, MNRAS, 335, L84
Tolstoy, E., Venn, K. A., Shetrone, M., Primas, F., Hill, V., Kaufer, A, & Szeifert, T. 2003, AJ, 125, 707 617, L119
Tolstoy el at., 2004, ApJ, 617, L119
Vader., J. P. 1986, ApJ, 305, 669
Vader., J. P. 1987, ApJ, 317, 128
Unavane, M., Wyse, R. F. G., & Gilmore, G. 1996, MNRAS, 278, 727
van der Marel, R. P., Alves, D. R., Hardy, E., & Suntzeff, N. B. 2002, AJ, 124, 2639 (vdM02)
Walcher, C. J., Fried, J. W., Burkert, A., & Klessen, R. S. 2003, A&A, 406, 847
Walker, M. G., Mateo, M., Olszewski, E. W., Bernstein, R. A., Wang, X., & Woodroofe, M. 2005, AJ, *in press* (astro-ph/0511465)
Westfall, K. B., Ostheimer, J. C., Frinchaboy, P. M., Patterson, R. J., Majewski, S. R., & Kunkel, W. E. 2006, AJ, 131, 375
Wilkinson, M. I., Kleyna, J. T., Evans, N. W., Gilmore, G. F., Irwin, M. J., & Grebel, E. K. 2004, ApJ, 611, L21
Xiao, W., Woodroofe, M., Walker, M., Mateo, M., & Olszewski, E. 2005, ApJ, 626, 145
Zaritsky, D., & Lin, D. N. C. 1997,AJ, 114, 2545

TABLE 1
RADIAL VELOCITIES OF STARS OBSERVED WITH MIKE[a]

Star	α_{2000}	δ_{2000}	UT Date	M_o	$(M-T_2)_o$	$(M-DDO51)_o$	RV_{helio}	RV_{gsr}	Q/σ	Cand?[b]	Member
C830356	6:35:11.95	–51:25:05.1	27Jan2004	18.84	1.30	–0.00	328.0	119.7	6	Y	N
C2520066	6:36:40.86	–51:58:07.0	27Jan2004	19.04	1.39	0.02	213.9	5.3	7	Y	Y
C2640634	6:38:22.77	–51:11:00.4	27Jan2004	18.08	1.62	0.01	221.2	12.2	7	Y	Y
C2680057	6:38:36.82	–51:16:23.9	28Jan2004	18.33	1.57	0.03	222.1	13.1	2.6	Y	Y
C2411078	6:38:47.04	–50:50:31.2	28Jan2004	18.65	1.42	0.04	229.4	20.4	4	Y	Y

[a] A full version of this table can be found in the electronic edition of the *Astrophysical Journal*.
[b] Denotes a photometric Carina giant candidate.

TABLE 2
RADIAL VELOCITIES OF STARS OBSERVED WITH VLT/FLAMES[a]

Star	α_{2000}	δ_{2000}	M_o	$(M-T_2)_o$	$(M-DDO51)_o$	RV_{helio}	RV_{gsr}	σ	Cand?	Member
C2501778	6:38:31.92	–51:07:04.8	19.76	1.22	0.01	230.3	21.3	2.9	2CD[b]	Y
C2680118	6:38:45.15	–51:11:26.6	19.56	1.20	0.02	216.3	7.2	2.6	Y	Y
C1400762	6:38:47.04	–51:00:46.8	18.60	1.27	–0.07	20.8	–188.2	1.1	CMD2[c]	N
C1401432	6:38:54.60	–51:04:01.2	20.17	1.19	0.05	216.8	7.7	7.6	Y	Y
C1402042	6:39:03.60	–50:57:43.2	20.63	1.91	–0.02	13.8	–195.3	2.1	CMD1[d]	N
C2413901	6:39:11.88	–50:58:40.8	19.28	1.31	–0.11	69.5	–139.7	1.0	N	N
C2413890	6:39:12.60	–50:54:10.8	19.68	1.19	0.02	225.0	15.8	3.4	Y	Y

[a]A full version of this table can be found in the electronic edition of the *Astrophysical Journal*.
[b]Denotes a star that is a 2CD outlier but lies inside Paper I giant box and within the Carina RGB selection.
[c]Denotes a star that lies just outside the RGB selection, but is a giant stars according to the Paper I selection criteria.
[d]Denotes a star that lies just outside the RGB selection, but is a giant stars according to the most conservative giant box used in this paper.

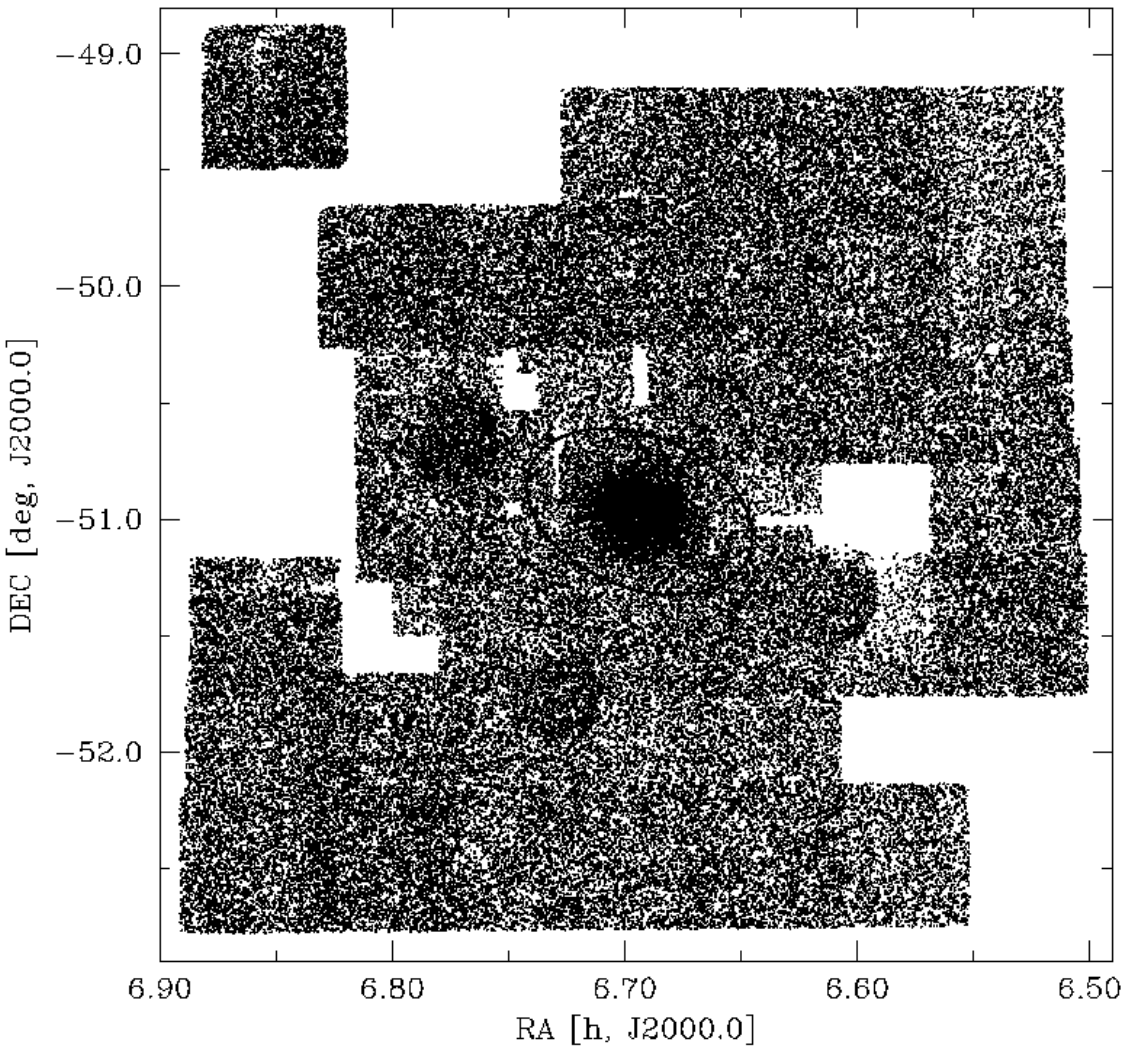

FIG. 1.— The area covered by our new photometric and spectroscopic survey. Points represent all stars in our photometric survey brighter than $M > 21$. The nominal King limiting radius of Carina from IH95 is delineated by the ellipse.

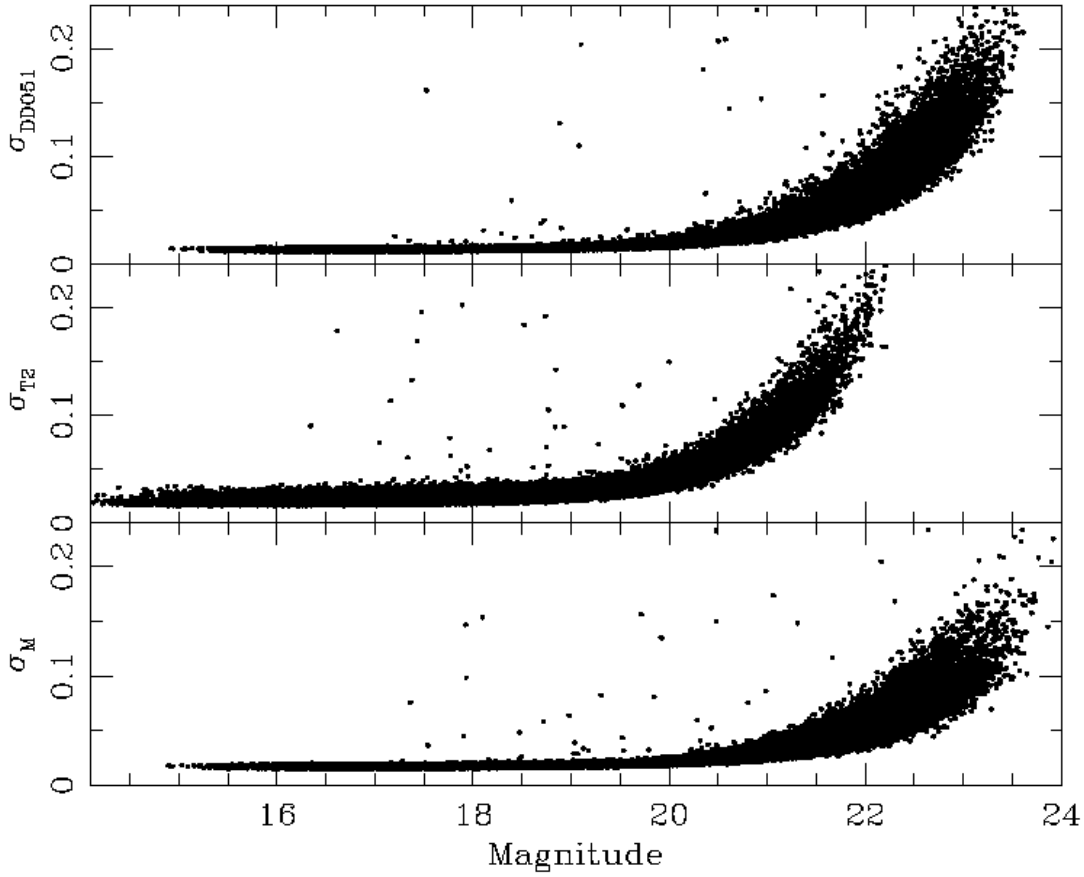

FIG. 2.— Photometric errors as a function of magnitude in our new Mosaic camera survey of the field centered on the Carina dSph.

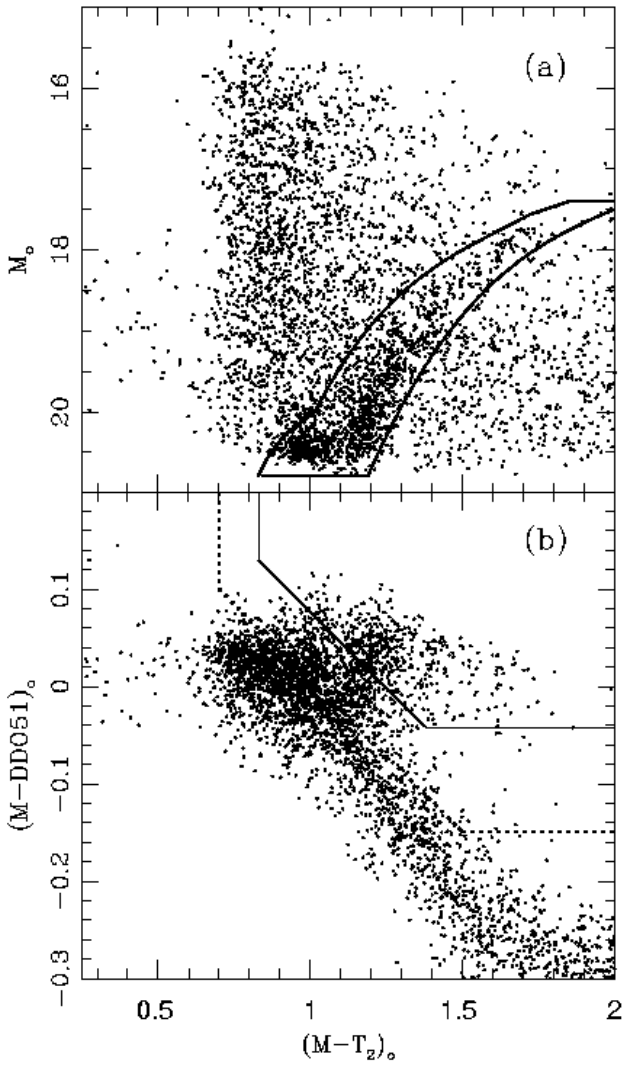

FIG. 3.— (a) The color-magnitude diagram of stars in our new Carina photometric survey. The solid line marks the region adopted to represent the Carina red giant branch. (b) The two-color diagram of stars in our Carina survey to $M = 20.8$. The solid line marks the region from which we pick stars likely to be giant stars. The dotted line delineates an expanded selection criterion used in Paper I and explored in §2.2 and §4.1. In both panels, only stars within one King limiting radius have been plotted as a guide to the general features of these distributions.

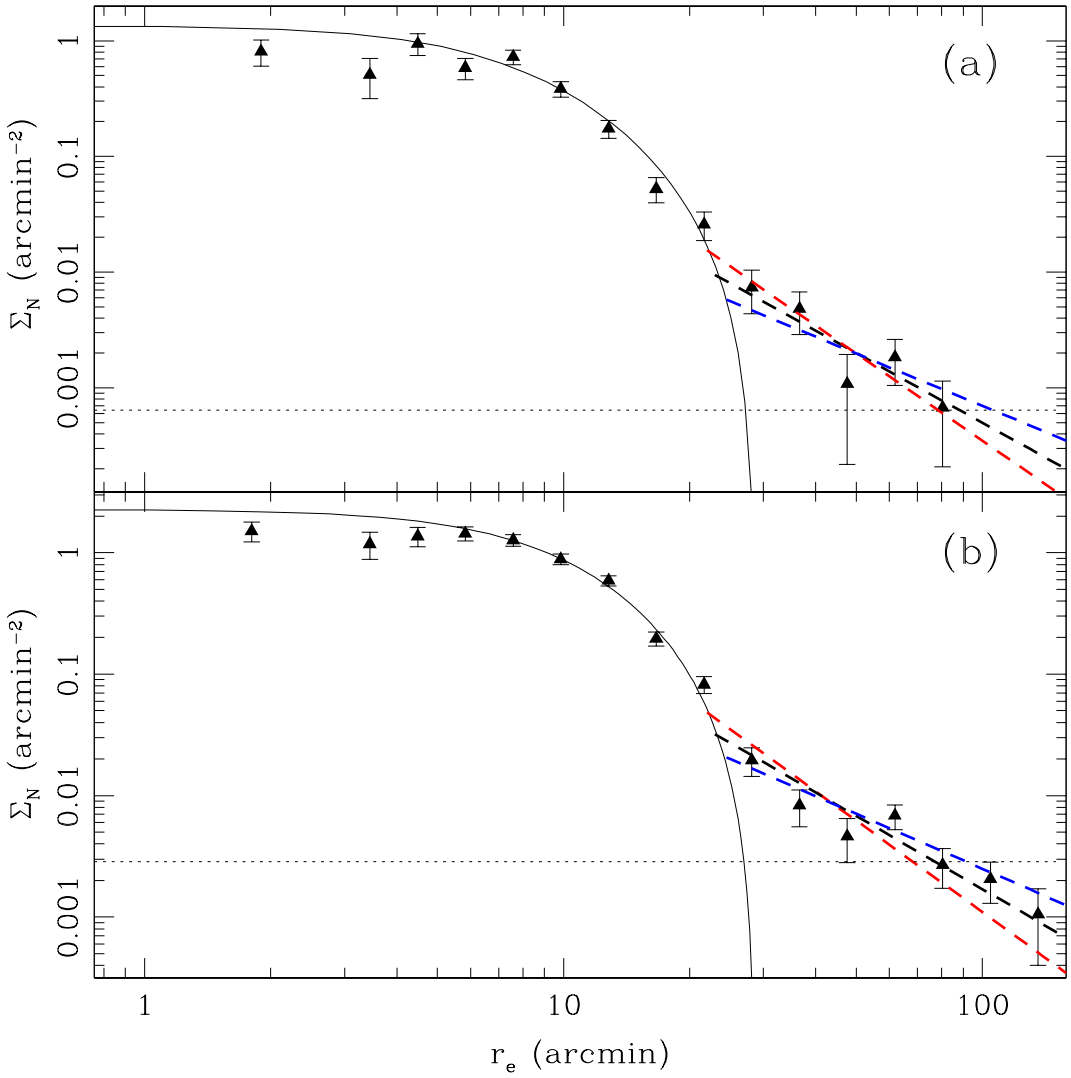

FIG. 4.— (a) The density profile derived for the Carina dSph using the $T_2 \leq 18.4$ sample. The dotted line shows the equivalent background density level that has been subtracted to produce the profile, as measured directly from the spectroscopic sample outside the nomimal King limiting radius (the ellipse shown in Figure 4, adopted from IH95). All stars have been binned into elliptical annuli according to the Carina ellipticity and position angle derived by IH95. Outside the IH95 King limiting radius, the density values shown come almost directly from the spectroscopically-confirmed Carina members from §3, which is 90% complete to $T_2 = 18.4$. (b) Same as panel (a) but for the $M \leq 20.8$ giant candidate sample. In this case, where we do not have spectroscopic coverage to the magnitude limit, we have subtracted the mean background level as derived by the method described in the text. The dashed lines in both panels show $r^{-1.5}$, r^{-2} and $r^{-2.5}$ power laws, while the curving solid line shows the IH95 King profile, scaled vertically to the density of our point at a radius of 10 arcmin.

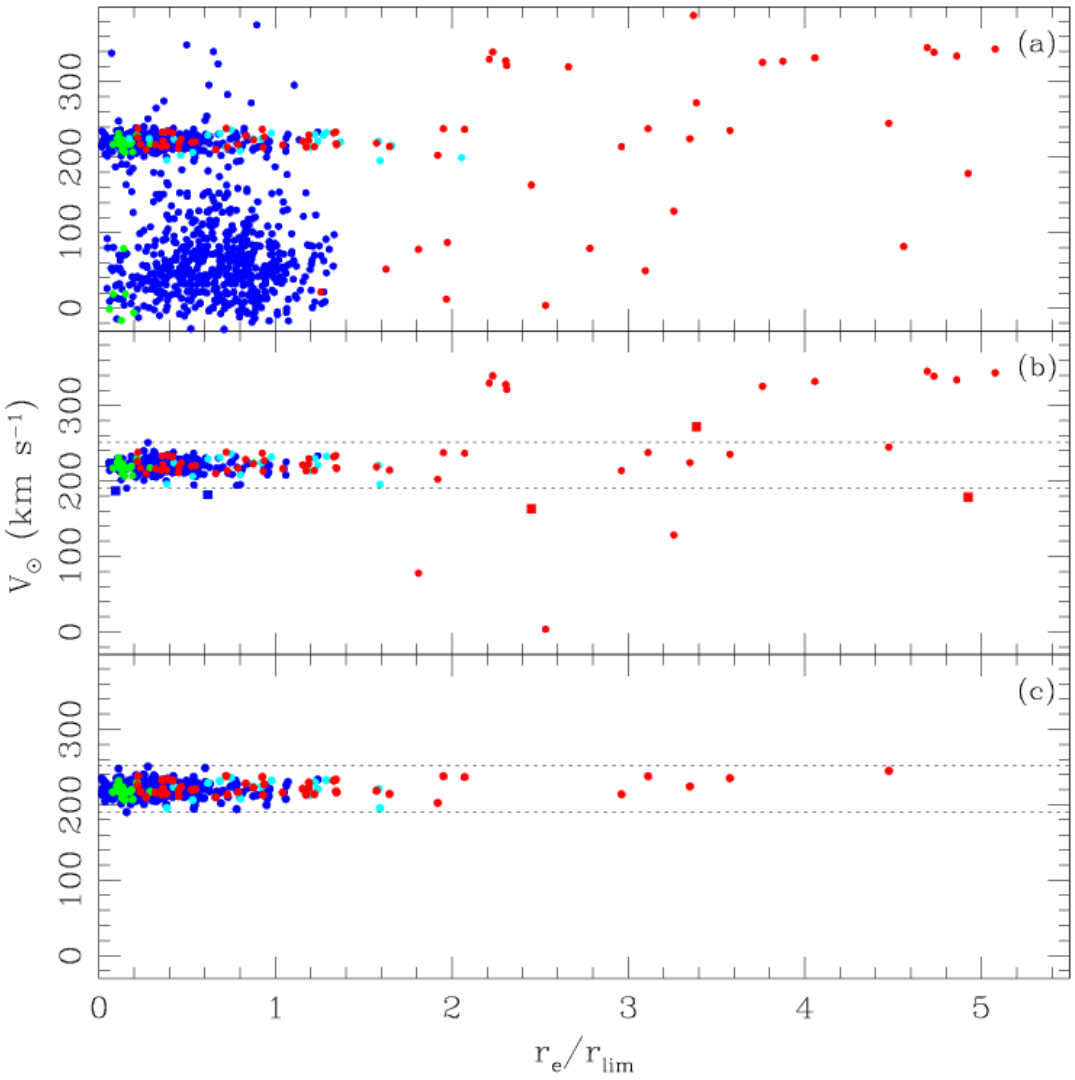

FIG. 5.— Distribution of derived RVs for the newly observed Carina giant candidates as a function of elliptical distance from the center of Carina. (a) All stars observed with MIKE (red), VLT+GIRAFFE (blue), Mateo et al. 1993 (green) and Carina giants from Paper VI (cyan). (b) Stars selected to be Carina giant candidates by our Washington+DDO5 photometry method and our CMD selection. The dotted horizontal lines mark the 3σ boundary used as our RV selection criterion. (c) RV distribution of our adopted final sample.

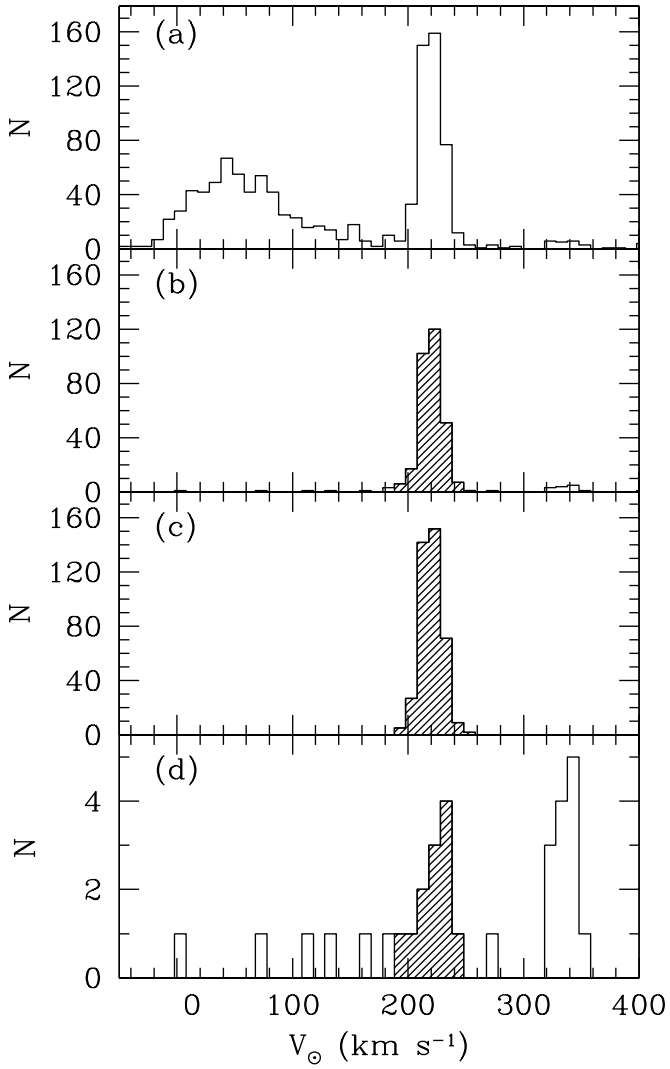

FIG. 6.— Histogram of the radial velocities for (a) all stars. This includes stars observed with MIKE, VLT+GIRAFFE, stars from Mateo et al. (1993) and Carina giants from Paper VI. (b) Stars that have been selected to be Carina giants by our photometric method. (c) Our final sample of Carina stars. (d) Histogram of stars selected as giant candidates having $r_e > 1.5 r_{lim}$ We have shaded the region whithin our RV selection criterion as shown in Figure 5.

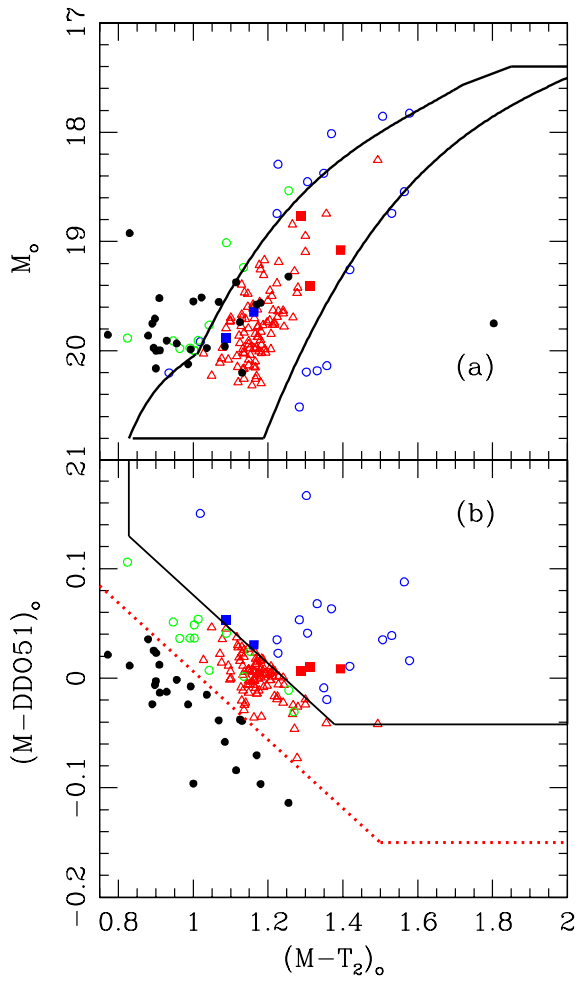

FIG. 7.— (a) Color Magnitude Diagram and (b) Color-Color Diagram for VLT+GIRAFFE stars with Carina-like velocities (as defined in Figure 5) that are not classified as Carina giants. Blue open circles mark stars that are CMD outliers, but that are classified as giant candidates by the more conservative criterion shown by solid lines in panel (b). Red open triangles show stars within the Carina RGB that were not selected as giant candidates by our conservative 2CD selection, but that are within the giant selection box defined in Paper I. Green open circles mark CMD and 2CD outliers by the conservative criteria of this paper but that would have been classified as giant candidates by the 2CD selection criterion adopted in Paper I. In addition, black circles show the CMD and 2CD position for stars with Carina-like velocities but that were not classified as giant by any of the above criteria. The figure also includes (as solid squares) the CMD and 2CD positions for the RV outliers discussed in §4.1.2 (blue squares for VLT+GIRAFFE examples and red squares representin examples from the MIKE data). See the text for more discussion.

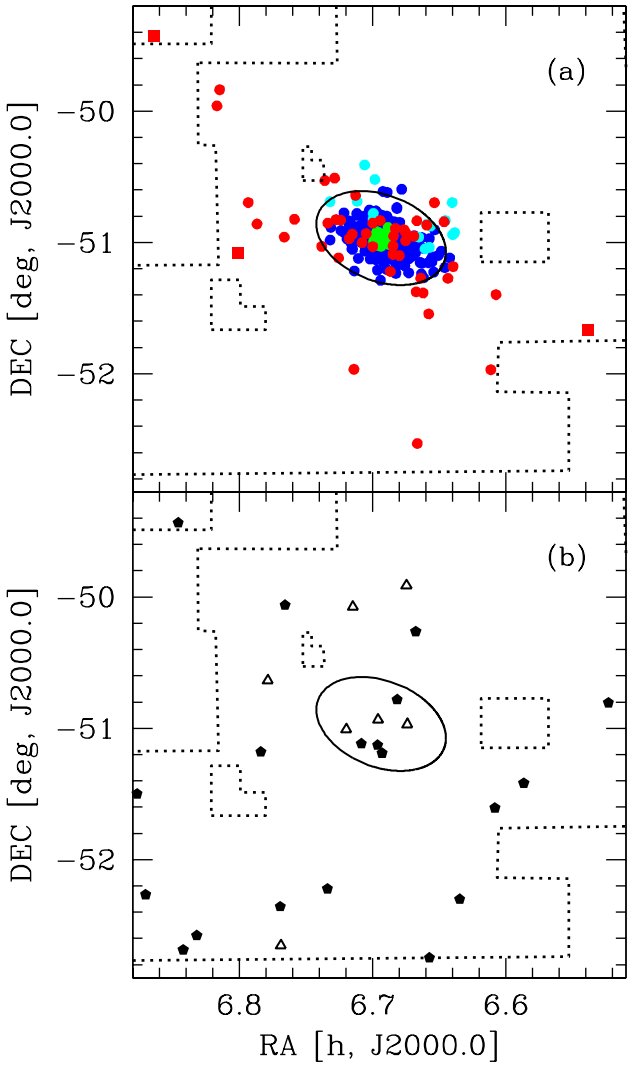

FIG. 8.— (a) Distribution of bona fide Carina RV-members on the sky. As in Figure 5, red circles show MIKE stars, blue circles mark VLT+GIRAFFE stars, green circles are stars from Mateo et al. (1993) and cyan circles mark stars whose RVs come from Paper VI. Shown also in the figure are the three red squared from Figure 5, which denote the three MIKE RV outliers discussed in §4.1.3. (b) The distribution of stars selected to be Carina giant candidates based on the CMD and 2CD that do not have Carina-like RVs is also shown. In particular, solid symbols mark the distribution of 332 km s^{-1} stars (see §6), and open symbols other RV outliers.

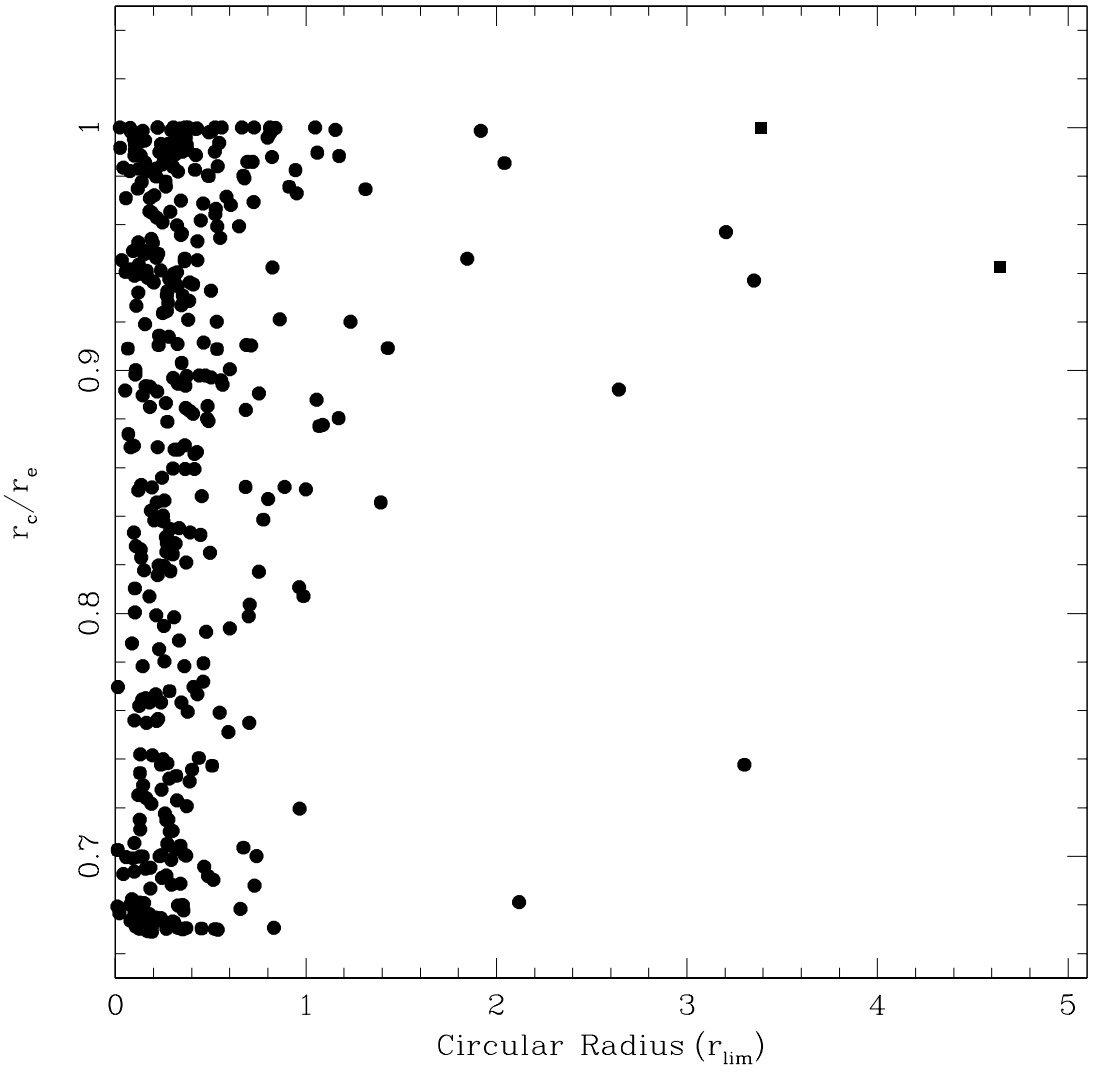

FIG. 9.— Ratio of the circular to elliptical radius for each Carina RV member versus circular radius. Stars on the major axis will have r_c/r_e=1 whereas stars on the minor axis will have r_c/r_e=0.67 (the ellipticity of Carina). The Figure shows that the mean r_c/r_e increases outward, indicating a preference of the stars to lie along the major axis.

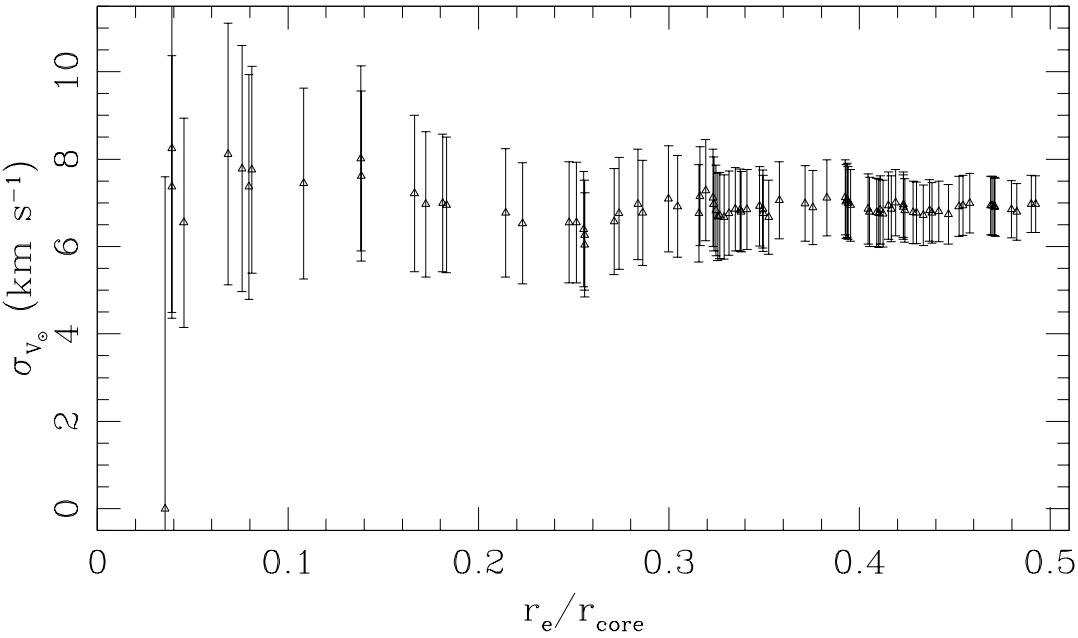

FIG. 10.— Central velocity dispersion as a function of radius expressed in terms of the King core radius. The dispersion is calculated so that stars are added one by one to the central bin (except the first point which includes the innermost three stars in the dataset) and using the maximum likelihood method. A value of 6.97 ± 0.65 km s^{-1} is reached at about half the core radius. The dispersion at this point includes the innermost 87 stars.

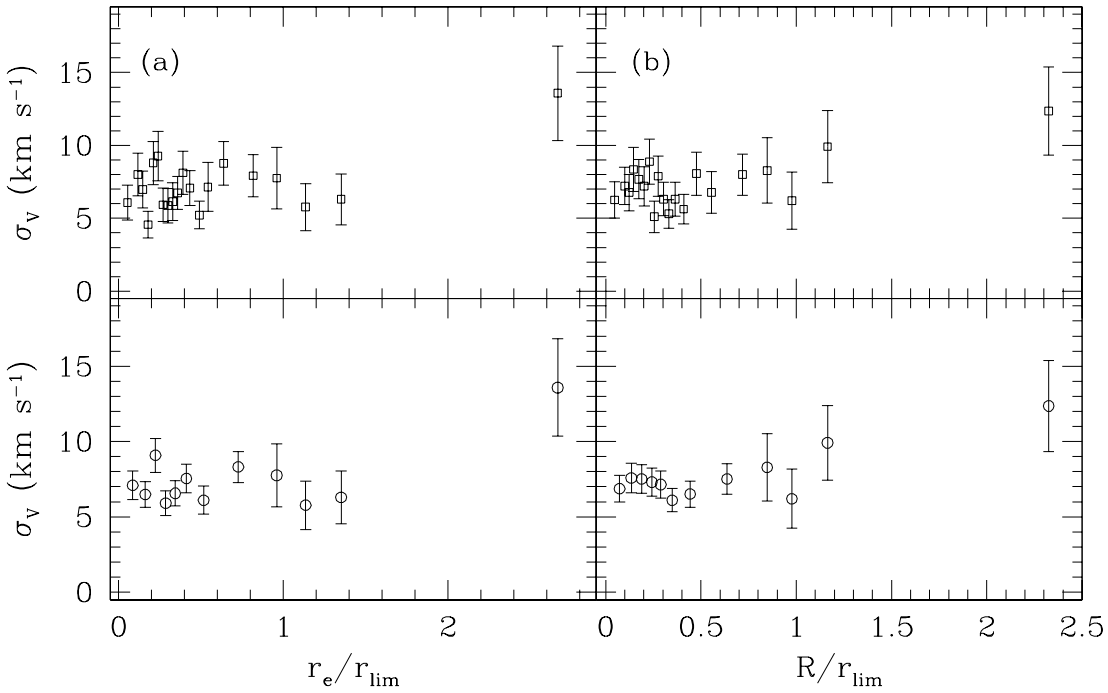

FIG. 11.— Velocity dispersion versus ellitical distance (left panels) and circular distance (right panels) for 23 and 46 stars per bin (lower and upper panels). To take into account the fact that the outer regions have a much lower density and therefore less stars are found there, the last four dispersion points in each panel were calculated with 10 stars each.

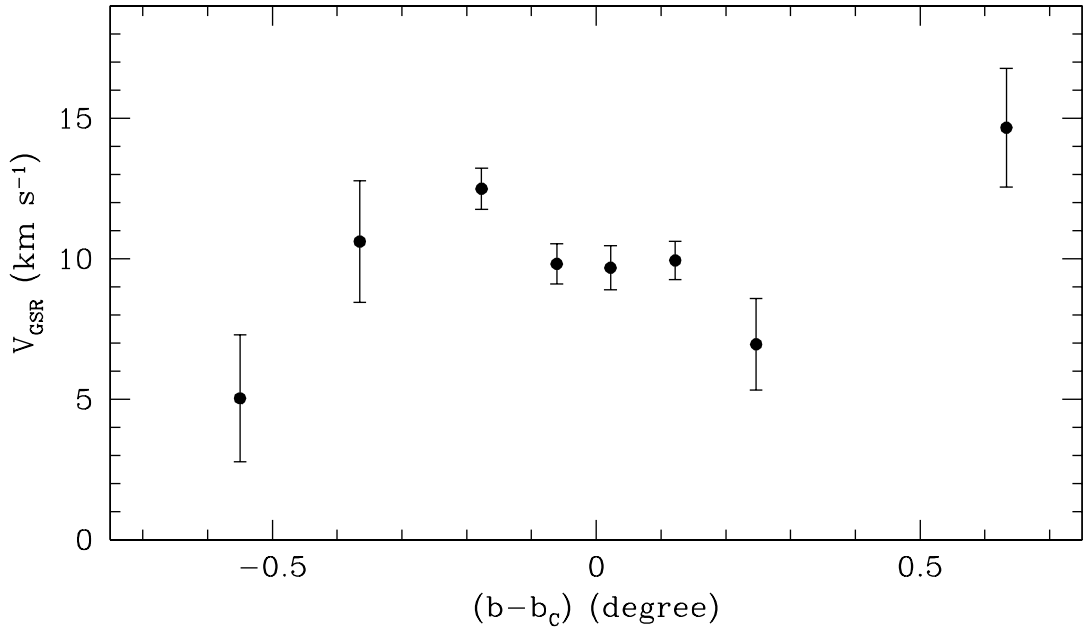

FIG. 12.— Mean Radial Velocity trend (in Galactic Standard of Rest) for the Carina dSph. The two outermost points on both sides from the center of Carina were calculated with 10 stars to take into account the lower density in the outer regions of the dSph. A peak-to-peak difference of ~ 10 km s^{-1} is observed over a 1.2 degree scale (2.1 kpc). We interpret this feature as indicative of tidal interaction.

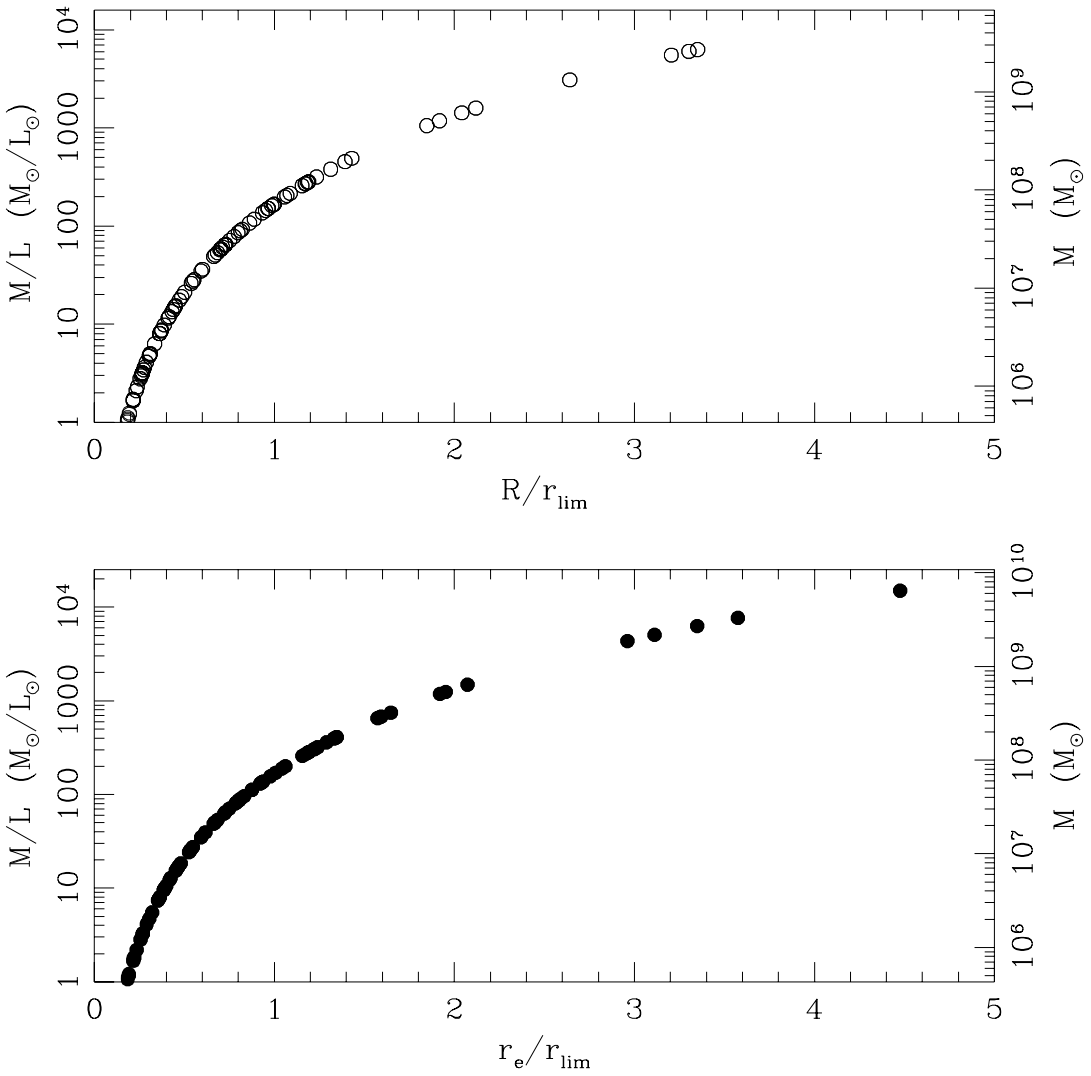

FIG. 13.— The implied global M/L implied for Carina as progressively more widely separated RV members are attributed as bound to the satellite. Open circles show the implied M/L of Carina assuming a spherical potential and the star's linear projected distance from the center of Carina. Solid circles show the M/L implied using *elliptical radii* on the major axis.

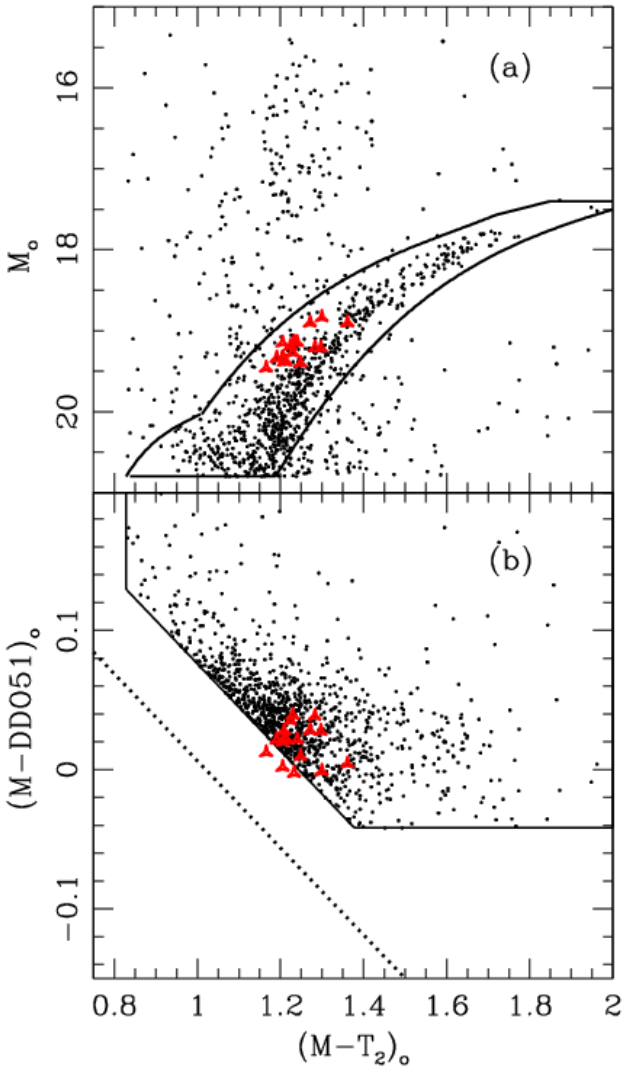

FIG. 14.— (a) Color-magnitude diagram of all giant candidates selected by the method in Figure 3b. The selection criterion applied to select Carina RGB stars from among all giant candidates is shown. Red triangles represent the 332 km s^{-1} moving group stars. (b) Color-color diagram corresponding to the CMD shown in (a). The Paper I giant box is also shown as dotted lines.

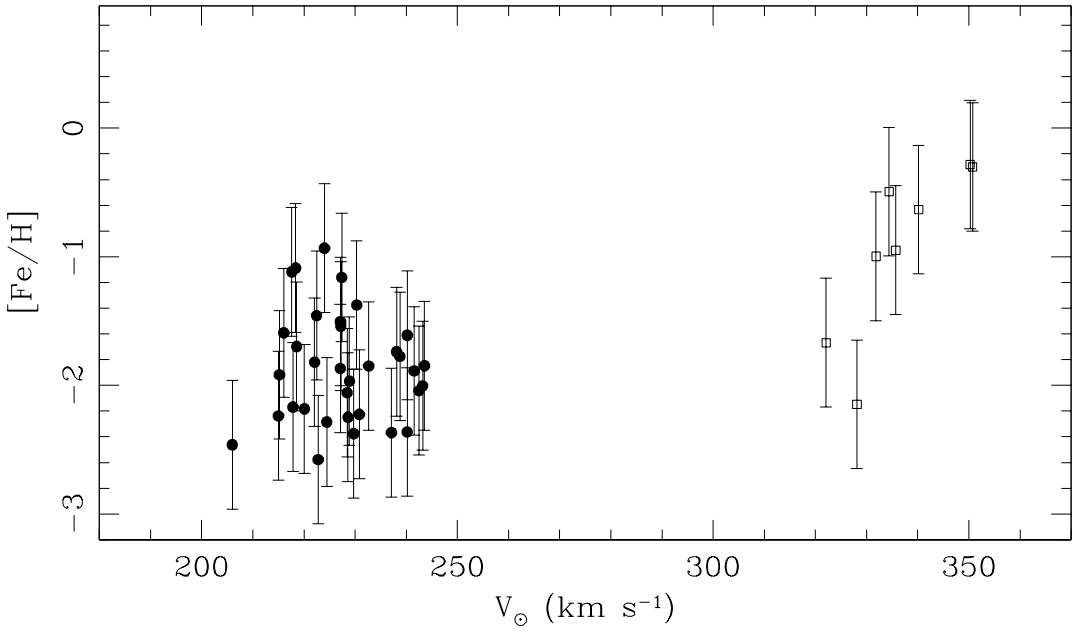

FIG. 15.— [Fe/H] from spectroscopic indices versus $V_{\odot}$. The new moving group stars are clearly more metal rich than the Carina stars, indicating that they might belong to a different population. The metallicities were calculated assuming that all the stars in the Figure are at the distance of Carina.

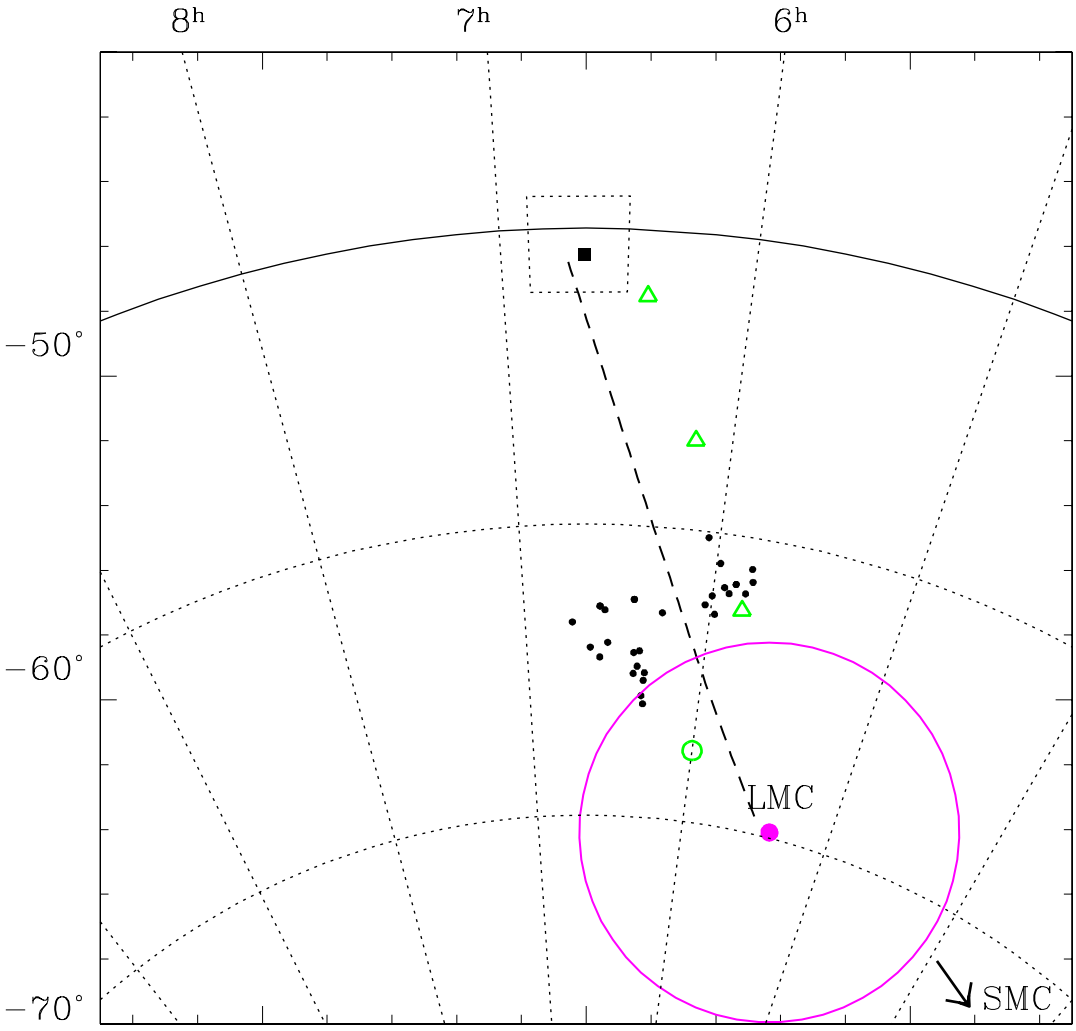

FIG. 16.— Map of the fields in which we have found stars with velocities like the LMC and the 332 km s^{-1} group. The position of the LMC is marked with a magenta circle while the large circle around it shows the 8° radius that marks the known extent of the disk. The dotted quadrangle around Carina (dSph center marked by the solid square symbol) shows the approximate extent of the current photometric survey (Fig. 1). Open green symbols show the location of other fields studied as part of a separate study of the LMC halo (Nidever et al., in preparation), with the open green circle closest to the LMC marking the field used to make the CMD and 2CD shown in Figure 18. The dashed line connecting the LMC with the Carina field marks a line of constant position angle between the two galaxies. The small black circles represent carbon stars in that region found by Kunkel et al. (1997a,b). The arrow points toward the center of the Small Magellanic Cloud.

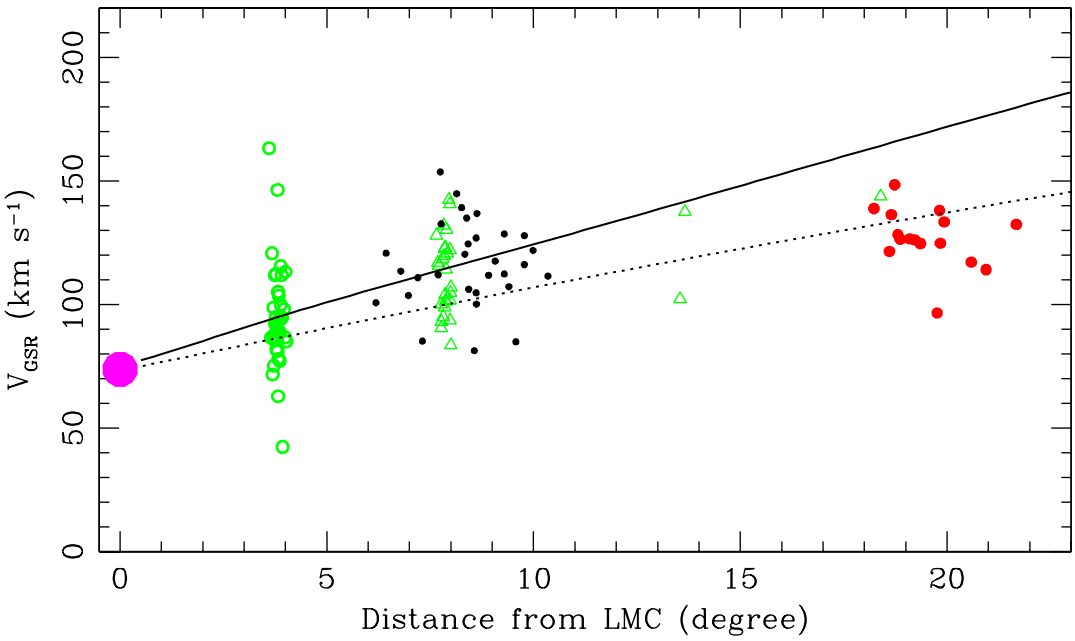

FIG. 17.— Velocity trend for stars observed in the periphery of the LMC and in the direction of Carina as a function of Galactic longitude and latitude. The LMC is indicated by the big solid symbol at $V_{GSR} \sim 75$. Red filled circles show the 332 km s^{-1} group observed with MIKE and GIRAFFE, open green triangles, open green circles and black dots correspond to stars in the fields marked with the same symbols in Figure 16. The dashed/solid line shows the velocity trend expected for the halo/disk of the LMC extrapolated to the distance of Carina (vdM02).

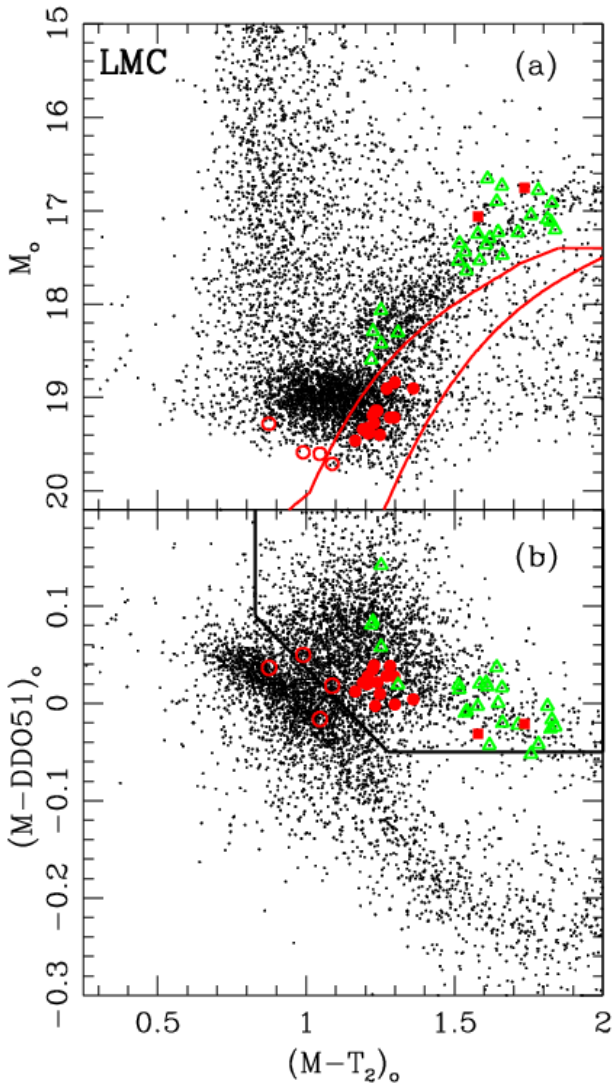

FIG. 18.— Color-magnitude diagram and color-color diagram for the field in the periphery of the LMC shown as the green open circle in Figure 16. The red lines mark the RGB selection box of Carina. The red circles represent members of the 332 km s^{-1} group found in the Carina field, with solid circles marking those stars observed with MIKE that satisfied our *Carina* selection criteria and the open red circles those VLT+GIRAFFE stars with velocities consistent with membership in the 332 km s^{-1} group. The green triangles represent other Magellanic stars stars found in our separate LMC survey. The two red squares represent those two "Magellanic giant candidates" observed with MIKE in August 2005; both are found to have RVs consistent with membership in the 332 km s^{-1} group.